CRCLEME

Cooperative Research Centre for
Landscape Environments
and Mineral Exploration

CSIRO

OPEN FILE
REPORT
SERIES

GOLD CONCENTRATIONS IN THE REGOLITH AT THE MT JOEL PROSPECT, WESTERN AUSTRALIA.

D.J. Gray

CRC LEME OPEN FILE REPORT 222

November 2008

CRCLEME

(CRC LEME Restricted Report 119R / E&M Report 650R, 1999
2nd Impression 2008)

GOLD CONCENTRATIONS IN THE REGOLITH AT THE MT JOEL PROSPECT, WESTERN AUSTRALIA.

D.J. Gray

CRC LEME OPEN FILE REPORT 222

November 2008

(CRC LEME Restricted Report 119R / E&M Report 650R, 1999
2nd Impression 2008)

CRC LEME is an unincorporated joint venture between CSIRO-Exploration & Mining, and Land & Water, The Australian National University, Curtin University of Technology, University of Adelaide, Geoscience Australia, Primary Industries and Resources SA, NSW Department of Primary Industries and Minerals Council of Australia.

Headquarters: CRC LEME c/o CSIRO Exploration and Mining, PO Box 1130, Bentley WA 6102, Australia

The CRC LEME–AMIRA Project 504 "**SUPERGENE MOBILIZATION OF GOLD IN THE YILGARN CRATON"** was carried out over the period 1998 to 2001. Twelve reports resulted from this collaborative project.

CRC LEME acknowledges the support of companies associated with and represented by the Australian Mineral Industries Research Association (AMIRA), and the major contribution of researchers from CSIRO Exploration and Mining.

Although the confidentiality periods of the research reports have expired, the last in July 2002, they have not been made public until now. In line with CRC LEME technology transfer goals, re-releasing the reports through the **CRC LEME Open File Report (OFR) Series** is seen as an appropriate means of making available to the mineral exploration industry, the results of the research and the authors' interpretations. It is hoped that the reports will provide a source for reference and be useful for teaching.

OFR 217 – Characteristics of gold distribution and hydrogeochemistry at the Carosue Dam prospect, Western Australia – DJ Gray, NB Sergeev and CG Porto.

OFR 218 – Gold distribution, regolith and groundwater characteristics at the Mt Joel prospect, Western Australia – CG Porto, NB Sergeev and DJ Gray.

OFR 219 – Supergene gold dispersion at the Argo and Apollo deposits, Western Australia – AF Britt and DJ Gray

OFR 220 – Geochemistry, hydrogeochemistry and mineralogy of regolith, Twin peaks and Monty Dam gold prospects, Western Australia – NB Sergeev and DJ Gray.

OFR 221 - Supergene gold dispersion in the Panglo Gold deposit, Western Australia – DJ Gray.

OFR 222 – Gold concentration in the regolith at the Mt Joel prospect, Western Australia – DJ Gray.

OFR 223 – Gold dispersion in the regolith at the Federal Deposit, Western Australia – NB Sergeev and DJ Gray.

OFR 224 – Supergene gold dispersion in the regolith at the Cleo deposit, Western Australia – AF Britt and DJ Gray.

OFR 225 – Distribution of gold arsenic chromium and copper in the regolith at the Harmony Deposit, northern Yilgarn, Western Australia – AF Britt and DJ Gray

OFR 226 – Supergene gold dispersion in the regolith at the Kanowna Belle and Ballarat Last Chance deposits, Western Australia – DJ Gray

OFR 227 – Supergene gold dispersion, regolith and groundwater of the Mt Holland region, Southern Cross province, Western Australia – AF Britt and DJ Gray.

OFR 228 – Supergene mobilization of gold and other elements in the Yilgarn Craton, *Western Australia* – ***FINAL REPORT*** – DJ Gray, NB Sergeev, CG Porto and AF Britt

This Open File Report 222 is a second impression (updated second printing) of CRC for Landscape Evolution and Mineral Exploration Restricted Report No 119R, first issued in November 1999. It has been re-printed by CRC for Landscape Environments and Mineral Exploration (CRC LEME).

Electronic copies of the publication in PDF format can be downloaded from the CRC LEME website: http://crcleme.org.au/Pubs/OFRSindex.html. Information on this or other LEME publications can be obtained from http://crcleme.org.au.
Hard copies will be retained in the Australian National Library, the J. S. Battye Library of West Australian History, and the CSIRO Library at the Australian Resources Research Centre, Kensington, Western Australia.

Reference:
Gray, D.J. 1999. Gold concentrations in the regolith at the Mt Joel Prospect, Western Australia. CRC LEME Restricted Report 119R, 44 pp. (Reissued as Open File Report 222, CRC LEME, Perth, 2008). Also originally recorded as CSIRO Exploration and Mining Restricted Report 650R, 1999.

Keywords: 1. Supergene gold 2. Mobilization of gold 3. Geochemistry 4. 3-D Modeling 5. Mt Joel Gold Prospect - Western Australia 6. Regolith

ISSN 1329-4768
ISBN 1 921 039 671

Addresses and affiliations of Authors:

D.J. Gray
CRC LEME
c/o CSIRO Exploration and Mining
PO Box 1130, Bentley,
Western Australia 6102.

Published by: CRC LEME
c/o CSIRO Exploration and Mining
PO Box 1130, Bentley, Western Australia 6102.

PREFACE

The principal objective of CRCLEME-AMIRA Project 504, *Supergene mobilization of gold and other elements in the Yilgarn Craton*, is to determine the mechanisms of supergene/secondary depletion, enrichment and dispersion of Au and other elements, so as to improve selection of drilling targets and further optimize interpretation of geochemical data. Extensive regolith investigations at Mt Joel have been previously documented, and this report describes further studies on the calculations of Au concentrations in regolith and bedrock at this site.

The Mt Joel prospect is situated in the northern part of the Yilgarn Craton, NE of Bronzewing. It is an area where the occurrence of supergene mobilization of Au is uncertain. Mt Joel consists of a number of mineralized targets in an area of relatively homogeneous geology, with highly variable regolith; in particular, the alluvial cover varies in thickness from less than one metre to greater than 80 m. For these reasons, this prospect provides a valuable study site for enhancing our knowledge of regional differences affecting the mobility of Au. Developing methods for the recognition and understanding of any such mobilization of Au, and potential pathfinder elements, is of major importance for successful exploration. This report investigates Au concentration and the type and degree of Au mobilization in the regolith and understanding the processes by which it occurs, using the software Mining Visualisation System (MVS). The Mt Joel site offers the possibility to compare Au concentration results from MVS (which is being used as a standard tool for a number of P504 site studies) with calculations based on raw data (which are not commonly feasible at other sites). Additionally, five Au prospects within the Mt Joel area which show contrasting regolith characteristics and differing thicknesses of transported cover are compared.

D.J. Gray,
Project Leader.
November , 1999

EXECUTIVE SUMMARY

Supergene gold mobility has been investigated at the Mount Joel prospect 20 km NE of the Bronzewing Au mine in the Yandal greenstone belt, Western Australia. Gold mineralization has been delineated along an 8 km long trend, primarily hosted in variably sheared and hydrothermally altered metabasalts. Gold occurs in a sulphide-poor quartz stockwork vein system associated with slightly anomalous concentrations of As, Sb and W. The area is generally flat and with a regolith cover of up to 100 m, including a variable thickness of alluvial cover.

Five mineralized zones, namely the 3000, 2400, 1600, 800 and 0 mN prospects, were investigated at the Mt Joel prospect. In the 2400 and 3000 mN prospects the saprolite is about 60 m thick and its upper portion is strongly leached, resulting in a Au-leached zone which is kaolinite rich. An alluvial cover less than 10 m thick overlies the saprolite. The cover and the top few metres of the saprolite are silicified. In comparison, in the 0 and 800 mN prospects, saprolite is commonly less than 30 m thick, more ferruginized and does not contain a leached zone. Above that, laterite residuum, up to 10 m thick, is present with a pisolitic zone at the top. This is overlain by palaeochannel sediments up to 80 m thick. The 1600 mN prospect has a similar thickness of transported material.

This report documents MVS calculations of regolith and rock Au concentrations at these five Mt Joel Au prospects. Comparisons with previous studies which used raw data show generally excellent agreement, particularly when data are viewed as a function of depth. However, the MVS data tend to be smoother than the raw data, possibly reflecting averaging across the sample area. In addition, the MVS values are proportionally lower than the raw values, most probably reflecting the drilling bias of the raw data. The MVS method appears less effective at matching high contrast boundaries, such as the Au-enrichment at the unconformity, although the interface enrichment is still obvious from the MVS calculations. There is little improvement in data quality at higher resolution, and this minor problem is postulated to be primarily due to the difficulty of extrapolating regolith boundaries and Au concentrations into areas with low drilling density.

The major features observed from the results of the five Mt Joel sites are:

(i) major vertical variability in Au concentrations, presumably prior to weathering;
(ii) residual enrichment of Au in the transition zone, by approximately 50 – 100%;
(iii) a relatively Au-poor zone within the upper oxide at the 3000 and 2400 mN prospects. The base of this zone varies from 450 mRL for the 3000 mN prospect to 432 mRL for the 2400 mN prospect. This variation is significantly greater than any variation in regolith boundaries between the two prospects, and appears to be primary;
(iv) a marked interface enrichment, most clearly observed for the 800 and 0 mN prospects where lateritic residuum has been retained;
(v) generally lower Au concentrations in the transported cover than in residuum. The highest Au concentrations in transported material occur in the 0 mN prospect, possibly because it is an area of greater palaeo-relief and the exotic transported material could be more readily contaminated by local sources of Au.

TABLE OF CONTENTS

LIST OF FIGURES

LIST OF TABLES

1 INTRODUCTION

1.1. Aim

The principal objective of CRC LEME-AMIRA Project 504, *Supergene mobilization of gold and other elements in the Yilgarn Craton*, is to determine the mechanisms of supergene/secondary depletion, enrichment and dispersion of Au and other elements, so as to improve selection of drilling targets and further optimize interpretation of geochemical data.

Within this framework, this report concludes previous investigations of the supergene distribution of Au at the Mount Joel Au prospect (Porto *et al.*, 1999) with calculations of Au concentration using the mining visualization system (MVS) program. This program is a useful tool for visualizing the three-dimensional patterns of Au distribution in the regolith and calculating degrees of depletion and enrichment.

1.2. Site description

The regolith geochemistry, stratigraphy and mineralogy at the Mt Joel Au prospect have been previously studied in detail (Porto *et al.*, 1999). The Mt Joel Au prospect is held by Great Central Mines Ltd. (GCM). It is located 20 km NE of the Bronzewing gold mine in the Yandal Greenstone Belt, about 400 km north of Kalgoorlie, latitude 27° 16' S and longitude 121° 13' E.

The mineralized trend at Mt Joel runs for about 8 km in a nearly N-S direction. Gold occurs in a quartz vein system hosted in metabasalts and amphibolites. Most of the Au is free, sometimes visible, but the vein system is generally sulphide-poor. The amphibolite grade mineral assemblage at Mt Joel overprints the tectonic fabric, implying that Au mineralization occurred before peak metamorphism and that the alteration envelop is metamorphosed (Phillips *et al.*, 1998).

Several mineralized zones have been detected at Mt Joel and are under evaluation, of which the 0 mN, 800 mN, 1600 mN, 2400 mN and 3000 mN prospects are discussed here. Nearly 1000 reverse circulation holes have been drilled in these zones in a 40 x 40 m grid pattern, locally closed to 20 x 20 m. The whole area is generally flat and deeply weathered. The regolith can be more than 80 m thick and a transported overburden is present, varying in thickness from a few metres in the centre and north of the study area to greater than 80 m in the south, where the residual profile is overlain by palaeochannel sediments. Regolith Au concentrations were calculated using a data base provided by GCM which included gold assay results and logging from exploration drilling. For each prospect, Au data were treated by MVS software. Graphical output of Au distribution were included in Porto *et al.* (1999), with the results from Au concentration calculations discussed in this report.

2 METHODS

Great Central Mines Ltd supplied logging and geochemical data for modelling using Mining Visualization System (MVS; © C Tech Corporation). Based on the logging data, four different regolith horizons were delineated:

(i) transported material, including alluvium and palaeochannel sediments;
(ii) oxide, which includes all *in situ* material down to the "base of complete oxidation" (BOCO; Section 3.2);
(iii) transition material, lying between the BOCO and the weathering front;
(iv) unweathered rock.

Five sites were studied, these being the 0 mN, 800 mN, 1600 mN, 2400 mN and 3000 mN prospects. The 0 mN, 800 mN and 1600 mN prospects are covered by up to 80 m of sediments, whereas transported cover is commonly less than 10 m for the 2400 mN and 3000 mN prospects.

Regolith boundaries (surface, unconformity, BOCO and weathering front) were gridded, "point" anomalies removed from the input data, and the data re-gridded. Although this filtering has the potential to bias the data, it was considered necessary to give coherent weathering horizons. For pictorial presentations of Au distribution, the data were pre-processed by logarithmic transform (base 10) of Au concentrations before gridding (Porto *et al.* 1999). Although this can affect the gridded magnitude of the main mineralization pattern, it enhances the detail of the subtle supergene redistributions. For Au concentration calculations, untransformed data were used.

The logged quartz concentration was also used for 3D modelling. The abundance of vein quartz (excluding silicification) was estimated during logging. This measurement is semi-quantitative, as quartz veining may be missed or over estimated if a sample is clay-rich and there may be variation between loggers. Data were treated in a similar way to the Au geochemistry, although logarithmic transforms were not used.

Stratigraphy was gridded with the KRIG_3D_GEOLOGY module within MVS. The kriging domain was confined to the region defined by the sample locations (convex hull), with the convex hull boundary offset to 0.05, maximum number of samples points set to 80, and other settings at default. Geochemistry was then kriged in relation to these surfaces, using the KRIG_3D module. The maximum number of data points (within the specified reach) that will be considered for the parameter estimation at a model node were set to 180, horizontal/vertical anisotropy set at 2.5 (data points in a horizontal direction away from a model node influence the kriged value at that node 2.5 times more than data points an equal distance away in a vertical direction), rectilinear offset parameter at 0.05, post-processing at maximum 2 ppm Au, and all other settings at default. The grid size used was X:Y:Z - 6.5 m:6.5 m:2.5 m.

Gold and quartz concentrations were calculated with untransformed data, using the VOLUME_AND_MASS module. No attempt was made to model different densities for different units. As the Au concentration data are as mass/mass rather than mass/volume, uniform density has only a minor influence on most calculations. The calculated concentrations do not compensate for leaching of mobile constituents: if half of the minerals have dissolved and been leached then Au concentration will double because of residual concentration.

In addition, (using the ISOVOLUME module) concentrations can be calculated for slices defined either by elevation (e.g., 390-393 m RL) or distance from a regolith boundary (*e.g.*, 3-6 m above the unconformity). Figure 1 illustrates nominal 3 m slices taken downwards from the surface and from the unconformity, which become truncated downwards by the unconformity and the base of

weathering, respectively. This occurs because the analysis is set up not to include the next regolith horizon. However, although this method may be arithmetically correct, it can lead to over- or under-estimations of concentrations as the slices get further from the reference boundary. This is because, ultimately, the slice being analyzed is incomplete, illustrated in Figure 1 as the slices becoming more and more truncated downwards by the base of weathering. Note that this is not a problem in calculation accuracy, but in the actual geometry of the study area. This can be expressed as a reliability factor, which is the mass of the slice divided by the mass of an untruncated slice (Figure 1). A reliability index of 85% indicates that the slice is 15% truncated.

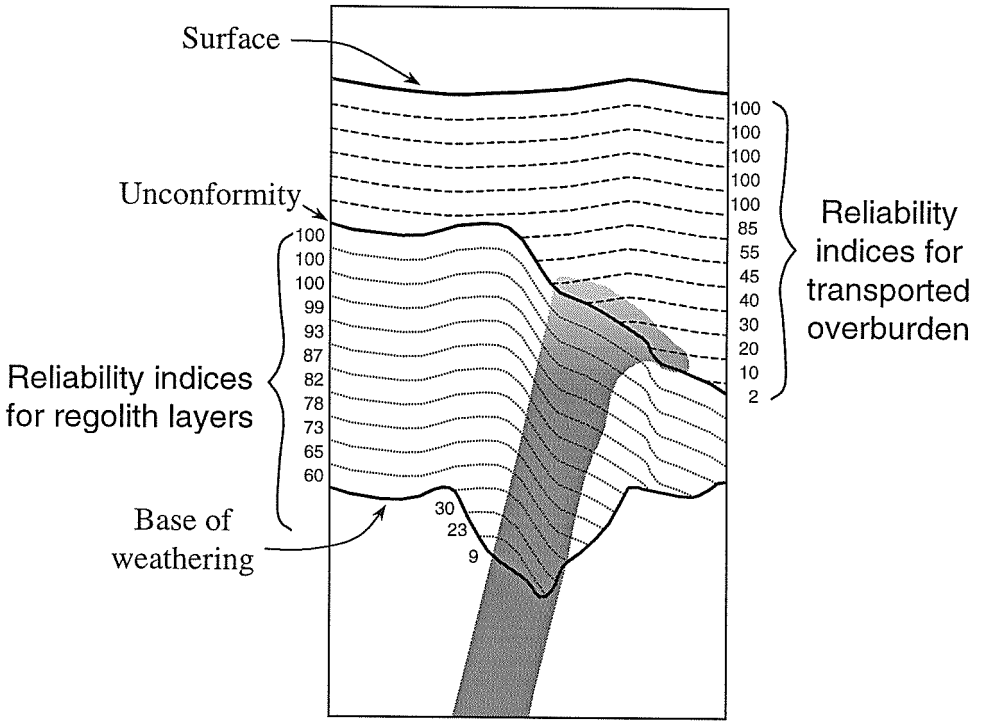

Figure 1: Diagrammatic representation of method of calculating Au concentration from slices defined for the upper surface and for the unconformity.

As the reliability index decreases, significant errors can occur. Figure 2 shows the results of Au concentration measurement for each slice in the residual regolith below the unconformity. Although the deeper slices are truncated (Figure 2a), they can still contain mineralized material, as in this example (Figure 1). Thus, a similar mass of Au is being divided by smaller and smaller amounts of regolith, which leads to anomalous Au concentrations (Figure 2b). In this example, the results indicate that the deepest slice has up to 440 ppb Au even though the "real" Au content is invariant at 80 ppb, except for the leached zone at the top of the *in situ* regolith.

When all the slices with reliability indices less than 60% are removed, the remaining results can be coded for reliability (Figure 2c). A much clearer picture of the Au trends is observed, illustrating the depletion at the unconformity. Note that this example is for the maximum possible overestimation of Au grade (the maximum overestimation = 100 ÷ reliability: *e.g.*, when reliability is 60%, maximum overestimation is 1.67; when reliability is 90%, maximum overestimation is 1.11). In other cases underestimation can occur for low reliability samples (due to truncated intersection with mineralization). In summary, those samples with reliabilities less than 80% are suspect (but can still be valuable if treated with caution), whereas those with reliability less than 60% should generally not be used.

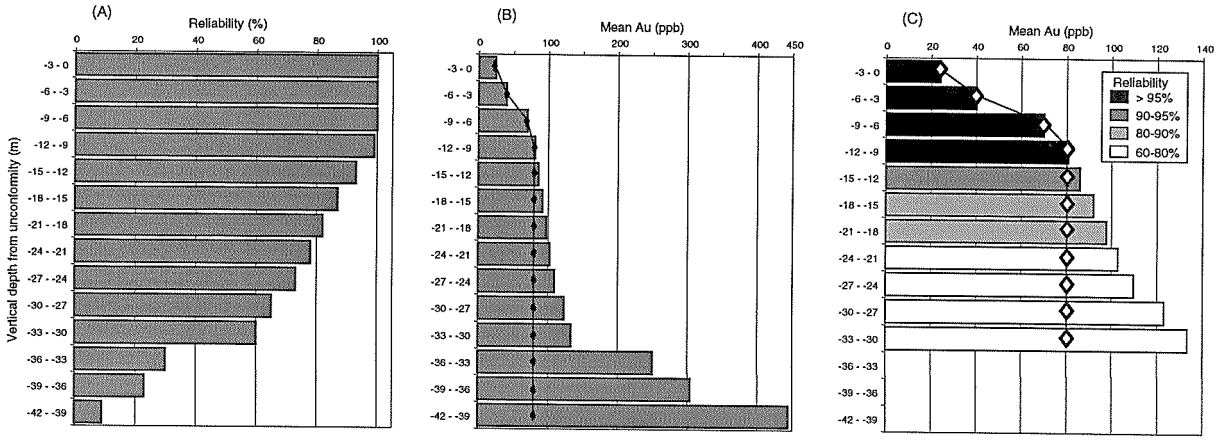

Figure 2: Calculated (a) regolith reliability, (b) unfiltered Au concentration and (c) filtered (> 60% reliability) Au concentration in residual regolith, colour coded to reliability. Diamonds represent expected Au concentration. Data based on situation represented in Figure 1.

Previously, MVS was used for modelling the regolith stratigraphy and the Au distribution in the regolith (Porto *et al.*, 1999). This report focuses on calculations of Au concentrations in the regolith and bedrock and comparisons with the quartz data.

3 REGOLITH STRATIGRAPHY

3.1 Introduction

This Section summarizes the major observations discussed in Porto *et al.* (1999) which are important for understanding of the results of the Au concentration calculations.

3.2 Regolith stratigraphy defined by Great Central Mines logging

Great Central Mines (GCM) defined three major regolith boundaries from visual observation of reverse circulation drill cuttings:

- Weathering Front - depth where the recovered material is totally constituted of fresh rock fragments.
- Base of Complete Oxidation (BOCO) - depth where the recovered material contains negligible unweathered rock fragments.
- Unconformity - separates residual from alluvial materials.

These boundaries separate four horizons: fresh rock; transition; oxide and transported cover. The weathering front and BOCO boundaries are deeper along the mineralized zone (Figure 3). The transported cover is generally less than 10 m thick but in the southern portion of the area it may reach depths of over 100 m within a palaeochannel running approximately W - E.

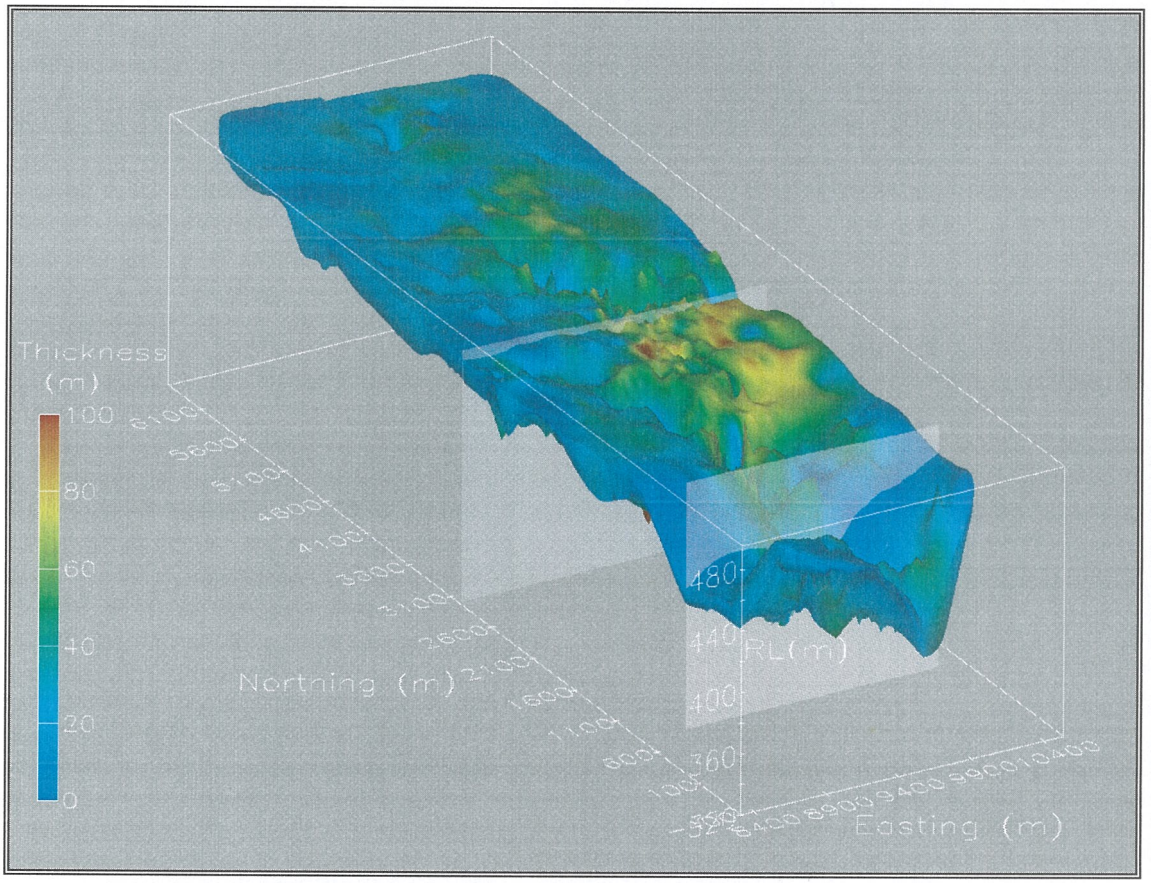

Figure 3: Thickness and elevation of the oxide horizon for the Mt Joel study area. Grey planes represent 800 and 3000 mN

3.3 Regolith stratigraphy defined by CRC LEME logging

Further regolith information derives from detailed logging of drill holes in sections 2920 mN, 3000 mN and 800 mN. The logging is based mostly on bulk colour of the samples, guided by the Munsell colour charts, and the nature of coarse fragments obtained by wet sieving of approximately 300 g of each sample.

SECTION 2920 mN (Figure 4):
The weathering front is commonly 100 m deep. Above it, a saprock unit has been defined based on the presence of relatively fresh biotite- and chlorite-bearing fragments with greyish colours. It coincides approximately with the transition horizon logged by GCM. The saprock grades up into the saprolite, the lower portions of which show paler colours from grey to orange. Upwards, the saprolite becomes more ferruginized and reddish brown. At depths of about 10 m the saprolite acquires a more uniform bright reddish brown colour due to a more uniform ferruginization. This is closely accompanied with silicification, which increases upwards and transgresses into the alluvial cover at a depth of 4 to 5 m. The transition to the transported cover is characterized by a change to orange colours, the presence of slightly rounded quartz grains and magnetic Fe nodules without cutans, and the general polymictic nature of the fragments.

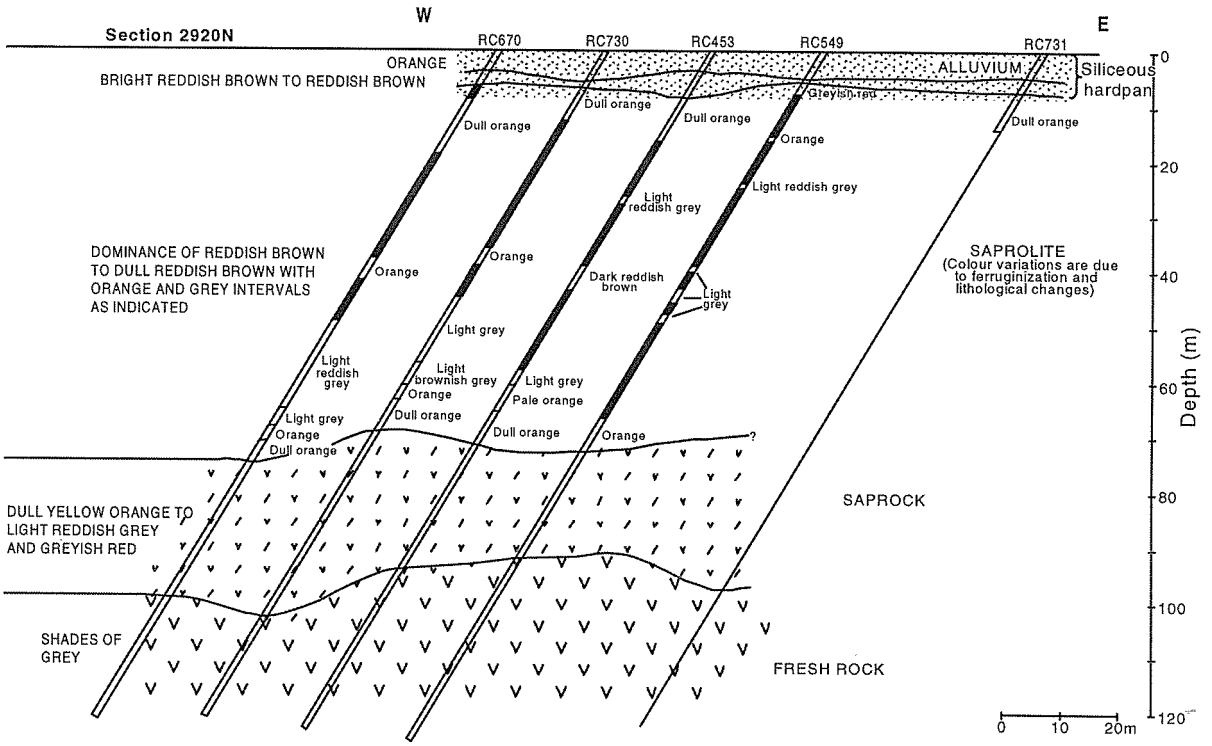

Figure 4: Regolith stratigraphy: Section 2920 mN

SECTION 3000 mN (Figure 5): Along this section the alluvial cover deepens to the east, in the direction of a palaeochannel and in this area the regolith stratigraphy is similar to the 800 mN prospect (see below). The unconformity separates lateritic residuum from palaeochannel sediments and the top of the lateritic residuum contains a layer with magnetic nodules and pisoliths, which grade downwards into a nodular horizon and then into a ferruginous saprolite. The western part of this section shows more significant (up to 10 m) differences between the GCM and CRCLEME logged unconformity.

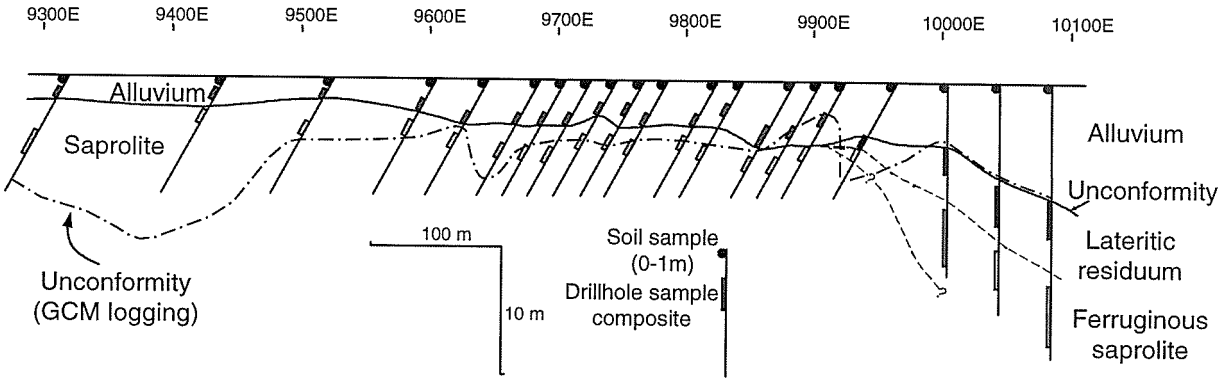

Figure 5: Regolith stratigraphy of section 3000 mN

SECTION 800 mN (Figure 6):
The regolith is dominated by a complete laterite profile overlain by 50 m of palaeochannel sediments. The saprock has similar characteristics to section 2920 mN but the saprolite could be more consistently divided into a lower pale portion and an upper ferruginous portion. The ferruginous saprolite grades upwards into a zone where yellow cutans develop over fragments of purple saprolite, forming a nodular structure in which the primary fabric is partly destroyed by ferruginization. Further upwards is a highly ferruginous zone with pisoliths, which are often magnetic, and where the saprolite fabric is completely destroyed. The transition to the palaeochannel sediments is characterized by the presence of a basal layer of grey clays grading upwards into a mottled clay zone and then into a predominantly red clay zone at the top. These clay zones contain no magnetic nodules or pisoliths but show slightly rounded quartz grains and rounded purple lithorelicts without cutans.

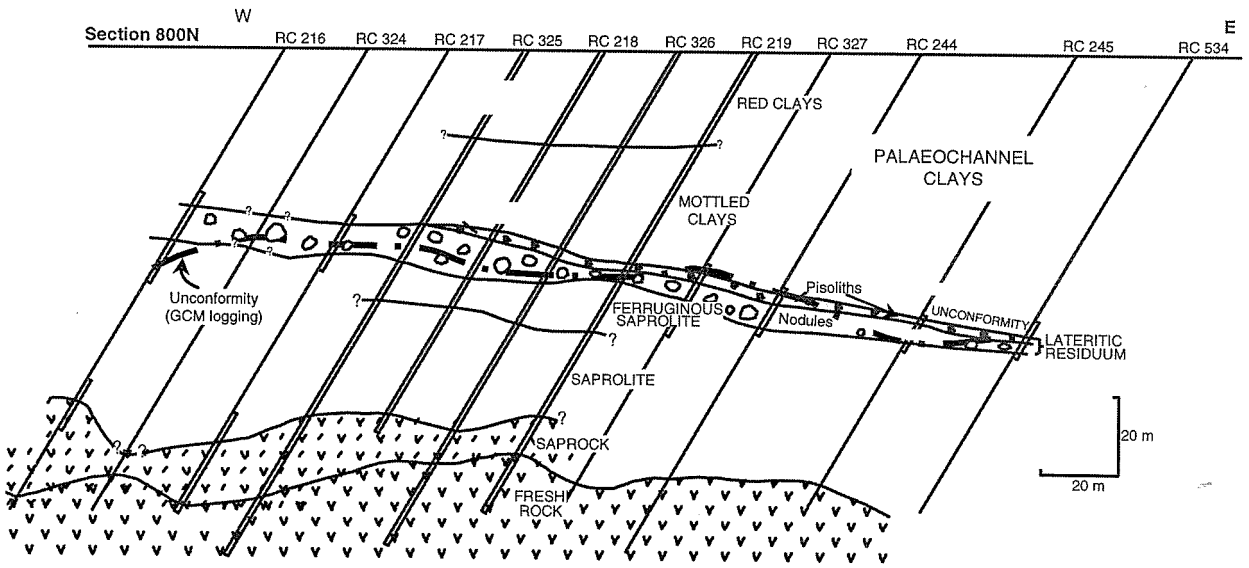

Figure 6: Regolith stratigraphy: Section 800 mN

3.4 Nomenclature used in this report

When referring to data generated by GCM, the terms used to refer to the regolith stratigraphy are transition, oxide and alluvium as shown in the first column of Table 1. The surfaces that separate these horizons are the Weathering Front, Base of Complete Oxidation and Unconformity. The logging terms used for the CRC LEME logging are shown in the third column of Table 1).

Additionally, in the prospects dominated by saprolites and covered by thinner alluvium, such as the 2400 mN prospect and most of the 3000 mN prospect, the saprolite (CRC LEME) / oxide (GCM) was further subdivided based on results of mineralogical, geochemical and Au concentration distribution patterns. The terms applied are shown in the second column of Table 1 and a brief justification for this subdivision is presented below but will become more apparent when results are presented in Section 4.2:

(i) *Top of saprolite*:
The topmost few metres of the saprolite, commonly silicified and/or ferruginized, and approximately coinciding with a distinct Au enriched zone;

(ii) *Au-poor zone*:
Occurring below the top of saprolite, to a depth of approximately 30 m (or 450 mRL), within which Au is distinctly lower;

(iii) *Lower saprolite*:
Saprolite below the leached zone and above saprock.

Table 1 compares the CRC LEME and GCM regolith terminology. However, it should be emphasized that although the transition horizon corresponds approximately to the saprock, and the oxide to the saprolite (and laterite where present), the position of the unconformity, as defined by GCM, tends to be recorded as 0 - 5 metres lower compared with the logging from this research. In Au concentration calculations of the raw data (Section 4) the lower 2 metres of the alluvium and upper 2 metres of the oxide (as defined by GCM logging) were combined as a defined "interface zone". For the calculations based on the MVS grids, 3 m either side of the unconformity was used. Due to the discrepancy in logging, this interface zone closely approximates the top of saprolite in the 2400 and 3000 mN prospects and the upper laterite in the 0 and 800 mN prospects (as defined by LEME logging; Table 1).

Table 1: Summary of the regolith stratigraphy terms used in this report, with approximate equivalencies between logging systems

GCM logging	CRC LEME logging	
	3000 mN prospect	800 mN prospect
Alluvium (with logged unconformity 0 – 5 m below that of LEME)	Alluvium	Alluvium (and palaeo-channel sediments)
Interface	Saprolite: Top of saprolite	Laterite pisolitic zone
Oxide: Au-poor zone	Au-poor zone	nodular zone
450 mRL → Lower oxide	Lower saprolite	Ferruginous saprolite Saprolite
Transition	Saprock	Saprock
Fresh rock	Fresh rock	Fresh rock

4 COMPARISONS OF CALCULATIONS BASED ON RAW DATA WITH MVS RESULTS

4.1 Introduction

The purpose of this Section is to check the validity of the Au concentration results obtained from the MVS calculations, by comparing these results with previous analyses conducted on raw data. Porto *et al.* (1999) combined the raw data into two groups in order to improve sample representation for their calculations: the 800 and 0 mN prospects were combined to represent areas with palaeochannel sediments overlying lateritic residuum, and the 3000 and 2400 mN prospects were combined to represent areas with thinner alluvial cover dominated by saprolite.

For each group of areas, several layers (2 to 10 m thick) are constructed upwards and downwards from the unconformity, BOCO and weathering front. Gold grades from the samples contained in those layers are used to determine arithmetic and geometric means.

Using MVS, Au concentrations in 3 m thick slices are calculated (Section 2). For the comparative exercise described below, these slices are combined to match the raw data layers as closely as possible.

4.2 Results for 3000 and 2400 mN prospects

The results for the 3000 and 2400 mN prospects are shown in Table 2, Table 3 and Table 4. The MVS arithmetic mean (hereafter denoted for simplicity as the MVS mean) shows a good linear correlation with the raw data arithmetic mean (hereafter denoted as the arithmetic mean or the ari-mean in plots) (Figure 7). The regression statistics are no poorer when the regression line is forced to intersect the origin. The lower values for the MVS mean, relative to the arithmetic mean is expected: the arithmetic mean represents biased data due to the greater density of drilling within the highly mineralized areas, whereas the MVS mean is an averaged mean across the entire prospect.

Table 2: Calculated Au concentrations based on the unconformity (3000 and 2400 mN prospects)

Raw data			MVS data	
Slice (m from unconformity)	Au (ppb) Arithmetic mean	Au (ppb) Geometric mean	Slice (m from unconformity)	Au (ppb) Arithmetic mean
+25 to surface	12	11	+ 24	3
+15 to 25	15	11	+15 to 24	6
+10 to 15	15	12	+9 to 15	14
+5 to 10	20	14	+6 to 9	21
+2 to 5	43	19	+3 to 6	28
0 to 2	77	25	0 to 3	40
0 to –2	88	28	0 to -3	47
-2 to –5	67	20	-3 to -6	45
-5 to –10	63	15	-6 to -9	41
-10 to –15	56	13	-9 to -15	42
-15 to –25	35	12	-15 to -24	34
-25 to –40	120	16	-24 to -42	72
-40 to BOCO	105	17	-42 to BOCO	84

Table 3: Calculated Au concentrations based on the BOCO surface (3000 and 2400 mN prospects)

Raw data			MVS data	
Slice (m from BOCO)	Au (ppb) Arithmetic mean	Au (ppb) Geometric mean	Slice (m from BOCO)	Au (ppb) Arithmetic mean
+30 to Unconf.	50	14	+ 30	52
+25 to 30	107	15	+24 to 30	101
+20 to 25	124	16	+21 to 24	126
+15 to 20	129	17	+15 to 21	137
+10 to 15	122	16	+9 to 15	137
+5 to 10	104	17	+6 to 9	133
0 to 5	120	19	0 to 6	132
0 to -5	122	22	0 to -6	139
-5 to -10	95	18	-6 to -9	144
-10 to -15	144	19	-9 to -15	140
-15 to -20	102	17	-15 to -21	120
-20 to -25	120	17	-21 to -24	106
-25 to BoW.	81	15	-24 to BoW	75

Table 4: Calculated Au concentrations based on the weathering front (3000 and 2400 mN prospects)

Raw data			MVS data	
Slice (m from weathering front)	Au (ppb) Arithmetic mean	Au (ppb) Geometric mean	Slice (m from weathering front)	Au (ppb) Arithmetic mean
+30 to BOCO	105	19	+ 30 to BOCO	67
+25 to 30	85	18	+24 to 30	89
+20 to 25	106	19	+21 to 24	91
+15 to 20	84	17	+15 to 21	84
+10 to 15	131	17	+9 to 15	86
+5 to 10	124	19	+6 to 9	86
0 to 5	98	17	0 to 6	78
0 to -5	69	15	0 to -6	73
-5 to -10	147	16	-6 to -9	76
-10 to -15	124	15	-9 to -15	68
-15 to -20	84	14	-15 to -21	79
-20 to -25	117	16	-21 to -24	73
-25 down	83	13	-24 down	49

Data based on relative distance from the unconformity (Figure 8) indicate, as discussed above, the arithmetic mean to be greater than the MVS mean. The geometric mean is lower still, despite being based on the raw data. This is as expected for a highly skewed data set. The difference between the arithmetic and geometric means declines at and above the unconformity, because the data are more normally distributed, due to Au remobilization close to the surface. When the raw data means are normalized (by dividing by 1.51) to match the MVS mean (Figure 9), the MVS and arithmetic mean show very similar depth trends, although the MVS changes are smoother than those for the arithmetic mean. The strong interface anomaly observed with the raw data means is more muted for the MVS means. This effect is discussed further in Section 4.3. Below the interface, Au contents are low for 20 m and are higher at the base of the oxide. As discussed above, the normalized geometric mean over-estimates Au content above the unconformity and under-estimates Au content for the more skewed data in the residual regolith. For simplicity, the geometric mean is not shown in further plots.

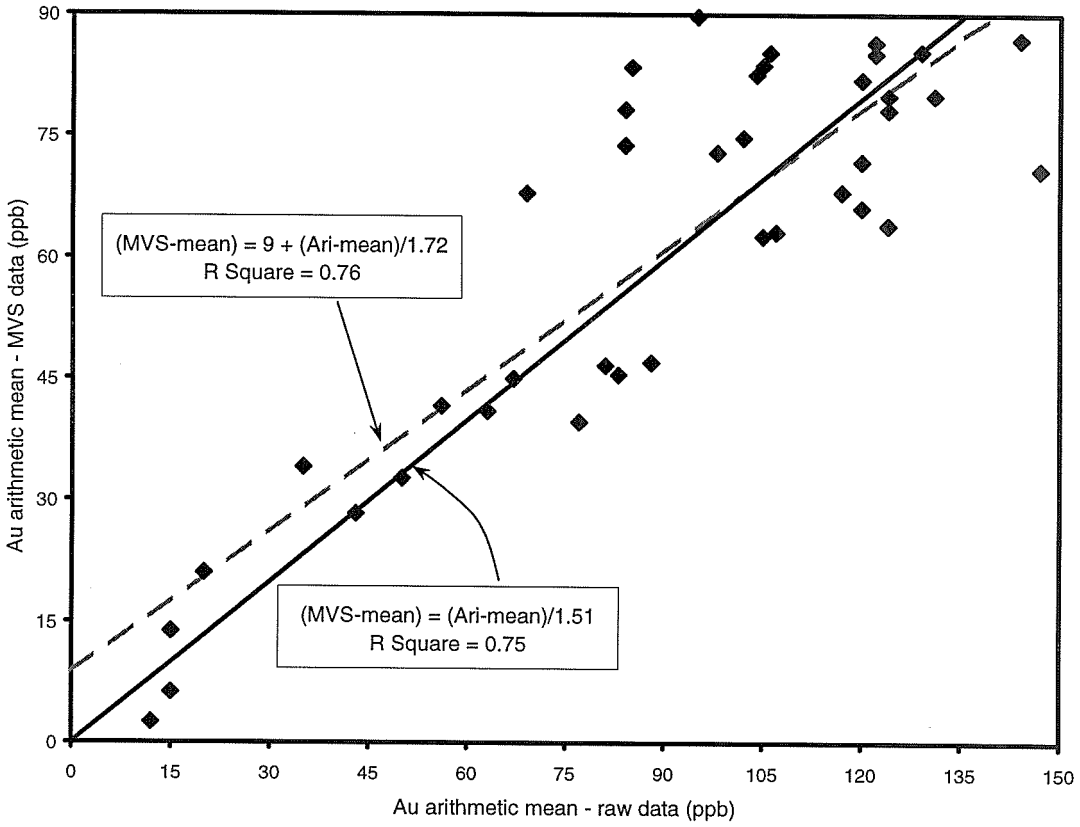

Figure 7: MVS mean vs. arithmetic mean for the combined 2400 mN and 3000 mN prospects

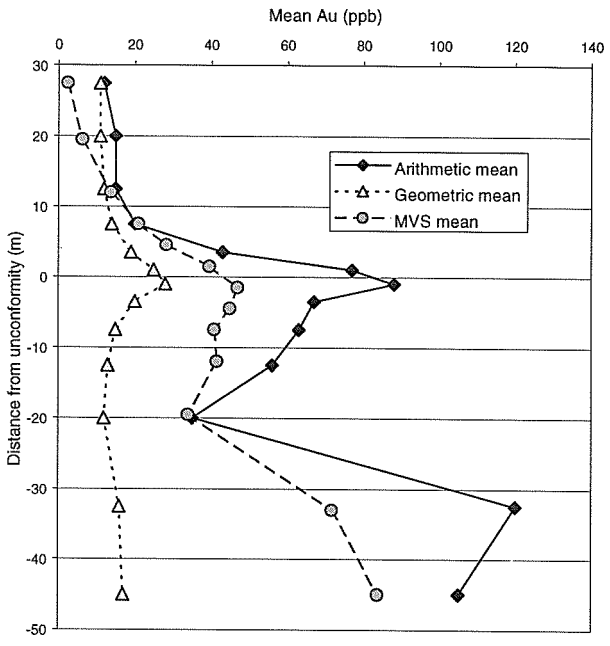

Figure 8: Calculated Au concentrations based on the unconformity (3000 and 2400 mN prospects).

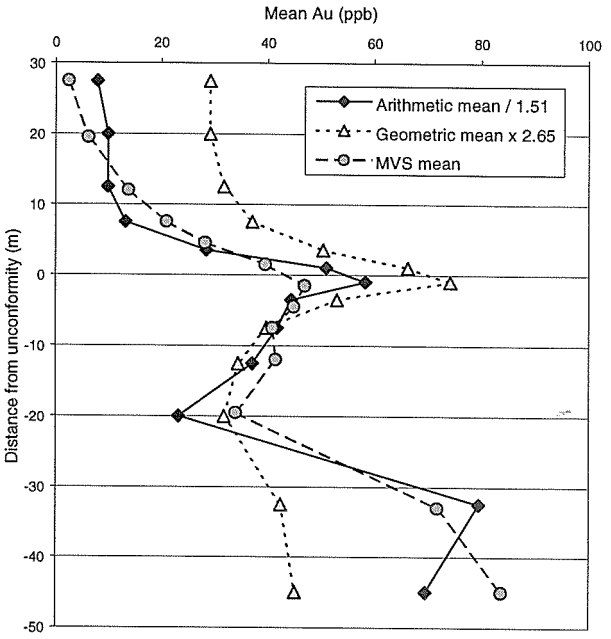

Figure 9: Calculated Au concentrations (normalized to the MVS mean) based on the unconformity (3000 and 2400 mN prospects).

These general patterns – low Au contents in the transported overburden; interface enrichment; moderate Au in the upper oxide; higher Au concentrations in the lower oxide – can also be observed in 3D Au distribution plots, as discussed for the 3000 and 2400 mN prospects in Sections 5.2 and 5.3. At both these sites the Au anomaly at the interface between oxide and transported materials is observed at a 50 ppb cut-off but is no longer visible when the cut-off is increased to 100 ppb (Figure 31 and Figure 46), consistent with the average grades at the interface indicated in Figure 9.

Results based on vertical distance from the base of complete oxidation (Figure 10) and the weathering front (Figure 11) show good agreement between the MVS mean and normalized arithmetic mean, with the MVS results being generally smoother. Twenty metres above the BOCO, Au concentration declines (Figure 10), consistent with a Au-poor zone in the upper part of the oxide, as discussed above. Compared to the fresh rock, there is only a minor increase in Au concentration in the transition, and this can be accounted for as an residual enrichment.

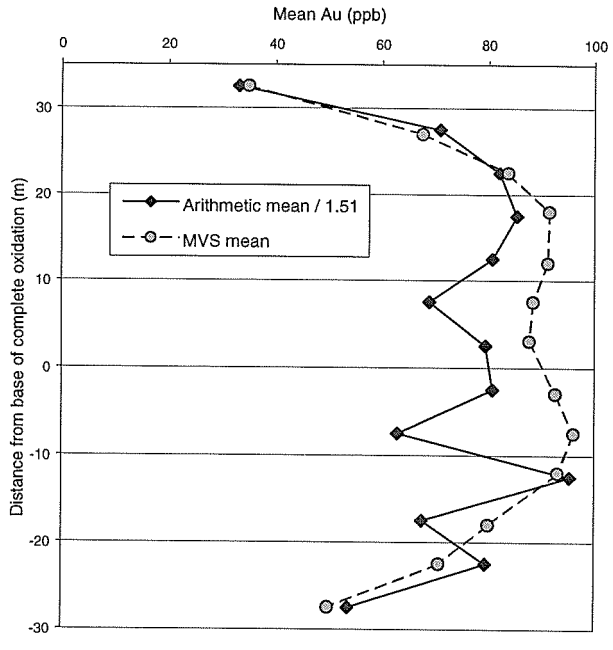

Figure 10: Calculated Au concentrations based on the BOCO surface (3000 and 2400 mN prospects).

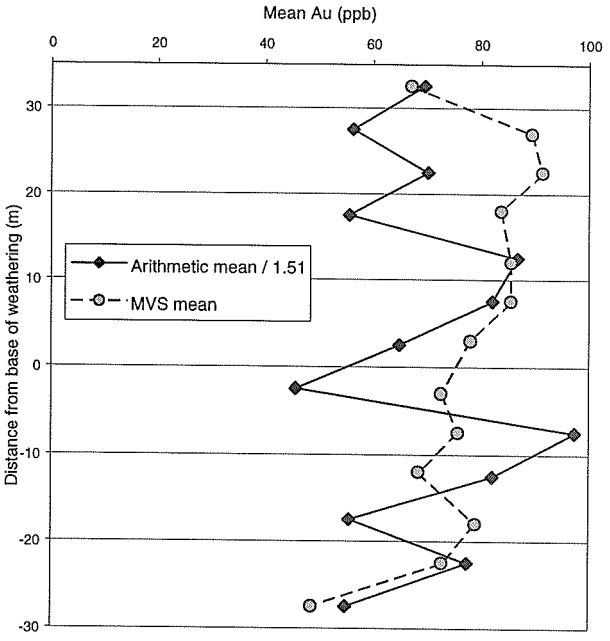

Figure 11: Calculated Au concentrations based on the weathering front (3000 and 2400 mN prospects).

4.3 Results for 800 and 0 mN prospects

The MVS means for the 800 mN and 0 mN have poorer linear correlation with the raw arithmetic mean (Figure 12) than for the combined 3000 and 2400 mN data (Figure 7). As shown in Tables 5, 6 and 7, the raw data values are approximately twice those of the MVS data, on average, compared to 1.5 x for the 3000 and 2400 mN prospects (Section 4.2). This greater difference between the raw and gridded data probably reflects differences in the geometries of the mineralization at the two areas. In the 3000 and 2400 mN prospects mineralization is broad and diffuse, whereas in the 800 and 0 mN prospects mineralization is more confined (compare Figure 31 and Figure 46 with Figure 77 and Figure 93). Greater bias in the data because of higher drilling density within the highly mineralized zone can be expected for the 800 and 0 mN prospects.

Table 5: Calculated Au concentrations based on the unconformity (800 and 0 mN prospects)

Raw data			MVS "normal" grid (3 m vertical spacing)		MVS "fine" grid (0.5 m vertical spacing)	
Slice (m from unconformity)	Au (ppb) Arithmetic mean	Au (ppb) Geometric mean	Slice (m from unconf.)	Au (ppb) Arithmetic mean	Slice (m from unconf.)	Au (ppb) Arithmetic mean
+40 to surface	14	10	+39 to surf.	11		
+25 to 40	12	11	+24 to 39	12		
+15 to 25	38	12	+15 to 24	17		
+10 to 15	33	12	+9 to 15	26	+10 to 15	25
+5 to 10	43	14	+6 to 9	45	+5 to 10	46
+2 to 5	120	20	+3 to 6	67	+2 to 5	75
0 to 2	226	32	0 to 3	90	0 to 2	94
0 to -2	205	35	0 to -3	97	0 to -2	99
-2 to -5	135	29	-3 to -6	88	-2 to -5	90
-5 to -10	93	19	-6 to -9	80	-5 to -10	76
-10 to -15	131	18	-9 to -15	63	-10 to -15	58
-15 to -25	78	16	-15 to -24	52		
-25 to BOCO	115	22	-24 to BOCO	58		

Table 6: Calculated Au concentrations based on the BOCO surface (800 and 0 mN prospects)

Raw data			MVS data	
Slice (m from BOCO)	Au (ppb) Arithmetic mean	Au (ppb) Geometric mean	Slice (m from BOCO)	Au (ppb) Arithmetic mean
+30 to Unconf.	152	24	+30 to Unconf	108
+25 to 30	123	17	+24 to 30	81
+20 to 25	35	13	+21 to 24	59
+15 to 20	103	20	+15 to 21	50
+10 to 15	124	26	+9 to 15	62
+5 to 10	115	22	+6 to 9	58
0 to 5	123	22	0 to 6	67
0 to -5	161	25	0 to -6	86
-5 to -10	167	24	-6 to -9	83
-10 to -15	137	25	-9 to -15	72
-15 to -20	119	24	-15 to -21	64
-20 to -25	198	26	-21 to -24	67
-25 to BoW	90	19	-24 to BoW	58

Data based on relative distance from the unconformity (Figure 13) indicate, as discussed above, the arithmetic mean to be greater than the MVS mean. As with the 3000 and 2400 mN prospects, the geometric mean is lower still, despite being based on the raw data. This is not unexpected for a highly skewed data set. The better agreement between the arithmetic and geometric means close to the surface is due to the data being more normally distributed, presumably due to Au remobilization. When the raw data means are normalized (by dividing by 2.06) to match the MVS mean (Figure 14), the MVS and arithmetic mean have very similar depth trends, although the MVS changes are smoother than those for the arithmetic mean. As with the 3000 and 2400 mN data, the raw data means show a stronger interface anomaly (also observed in 3D Au distribution plots; Figure 93) than the MVS means. To test whether this result is a function of grid resolution, the MVS means were recalculated using 0.5 m vertical grid spacing and 0.5 m vertical slices (Figure 14; "fine" grid data in

Table 5). The lack of enhancement indicates that the difference is due to other factors. One possible difficulty is accurately gridding the position of the unconformity in areas with little drilling data. However, it should be noted, that for both the 3000 and 2400 mN and the 800 and 0 mN areas, agreement between the raw data and MVS data is generally very good.

Table 7: Calculated Au concentrations based on the weathering front (800 and 0 mN prospects)

Raw data			MVS data	
Slice (m from weathering front)	Au (ppb) Arithmetic mean	Geometric mean	Slice (m from weathering front)	Au (ppb) Arithmetic mean
+30 to BOCO	120	23	+30 to BOCO	55
+25 to 30	251	26	+24 to 30	110
+20 to 25	268	32	+21 to 24	109
+15 to 20	173	31	+15 to 21	85
+10 to 15	117	26	+9 to 15	70
+5 to 10	152	24	+6 to 9	68
0 to 5	115	22	0 to 6	57
0 to -5	58	16	0 to -6	51
-5 to -10	108	19	-6 to -9	54
-10 to -15	64	18	-9 to -15	53
-15 to -20	129	20	-15 to -21	49
-20 to -25	183	19	-21 to -24	42
-25 down	43	12	-24 down	53

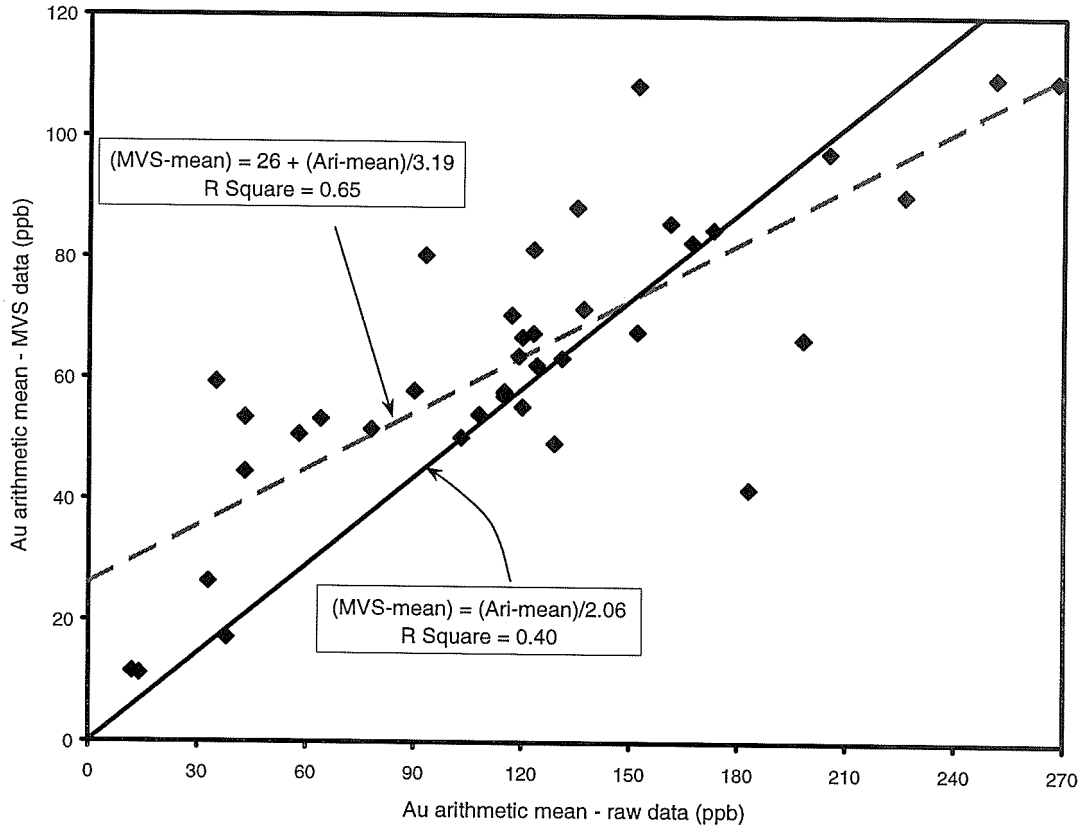

Figure 12: MVS mean vs. arithmetic mean for the combined 0 mN and 800 mN prospects

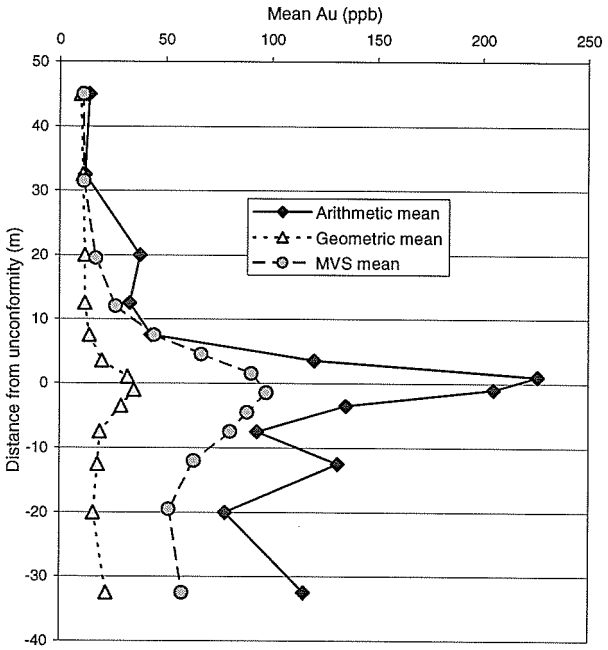

Figure 13: Calculated Au grades based on the unconformity (800 and 0 mN prospects).

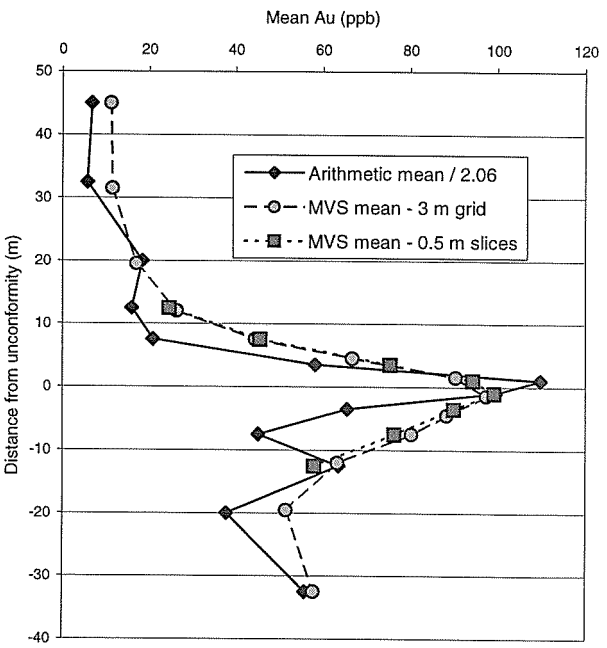

Figure 14: Calculated Au grades (normalized to the MVS mean) based on the unconformity (800 and 0 mN prospects), using "normal" and "fine" gridding and analysis

Changes in Au distribution across the BOCO surface and the weathering front are minor (Figure 15 and Figure 16), again with good agreement between raw and MVS means.

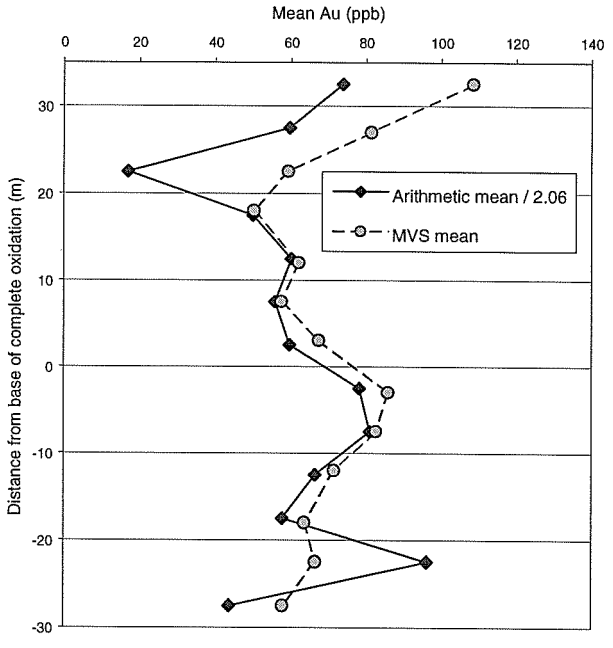

Figure 15: Calculated Au grades based on the BOCO surface (800 and 0 mN prospects).

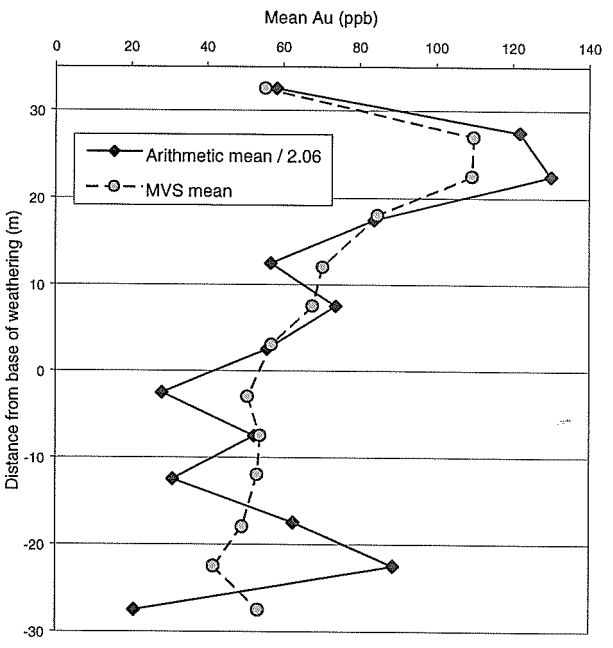

Figure 16: Calculated Au grades based on the weathering front (800 and 0 mN prospects).

4.4 Conclusions

The compiled results for both areas show a generally excellent agreement between raw data and MVS mean Au concentrations, particularly when viewed as a function of depth. The MVS data tend to be smoother than the raw data, reflecting averaging of data across the sample area. The proportionally lower Au concentrations from the MVS calculations, relative to the raw data, most probably reflect the spatial bias in the drilling. The MVS method appears less effective at matching high contrast boundaries, such as the Au-enrichment at the unconformity, although the interface enrichment was still obvious for the MVS calculated results.

5 GOLD CONCENTRATION RESULTS FOR EACH PROSPECT

5.1 Introduction

Gold concentrations and regolith volumes were calculated for each of the five mineralized prospects: 0 mN, 800 mN, 1600 mN, 2400 mN and 3000 mN. The spreadsheet data files for all cases are included in the accompanying CD. Each prospect will be discussed separately (Sections 5.2 - 5.6), with a comparison of results in Section 5.7, Table 8 to Table 9. The 3000 and 2400 mN and 800 and 0 mN prospects represent two distinct regolith environments. The 3000 and 2400 mN prospects have a truncated profile with thin (generally < 10 m) cover, whereas the 800 and 0 mN prospects were previously lowland areas and have complete profiles buried by up to 100 m of palaeochannel sediments and other transported overburden. In both areas, the weathering front and the BOCO have similar elevations.

5.2 3000 mN prospect

Calculations of the mean thicknesses of each regolith layer at 3000 mN (Figure 17) indicate a minor thickness of transported cover (7.5 m), a thick oxide (60 m) and a moderately thick transition to unweathered rock (27 m). Bedrock and transition have similar mean Au concentrations (103 ppb and (101 ppb Au, respectively; Figure 18), but there is significantly less Au in the oxide (58 ppb). As expected, the transported overburden is Au-poor (20 ppb). Vein quartz content is similar for the three *in situ* horizons, but is less in the alluvium (Figure 19). On the basis of the observations made previously (Section 4.2), the 3 m above and below the unconformity were combined as the *interface*, and the oxide horizon (less the top 3 m) split into > 450 mRL and < 450 mRL zones (Figure 20) to maximize the differences between the upper and lower oxide. This new division of the regolith indicates a Au-poor alluvium (15 ppb), over a slightly enriched interface (29 ppb). The upper section of the oxide has a much lower Au content (27 ppb Au) than the lower oxide (76 ppb Au; (Figure 21). Quartz content is also less in the upper oxide than below (Figure 22), although there is no interface enrichment. Correlation of low quartz with low Au would suggest that primary variability rather than weathering processes is the cause of the lower Au in the upper oxide.

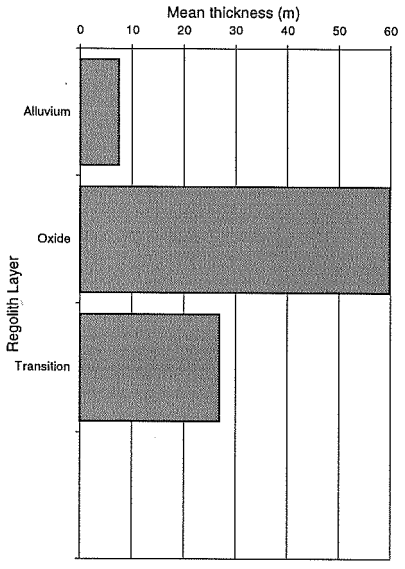

Figure 17: Mean thickness of each regolith layer from the Mt Joel 3000 mN prospect.

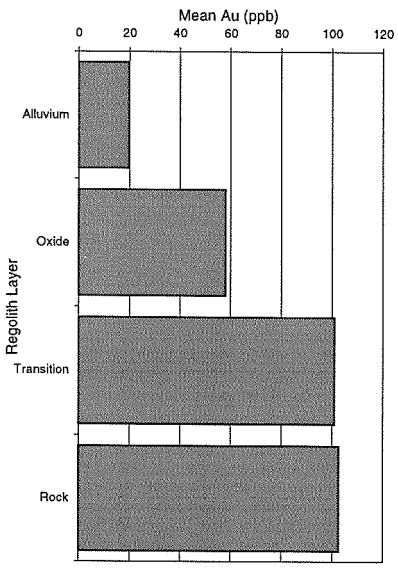

Figure 18: Mean Au for each regolith layer from the Mt Joel 3000 mN prospect.

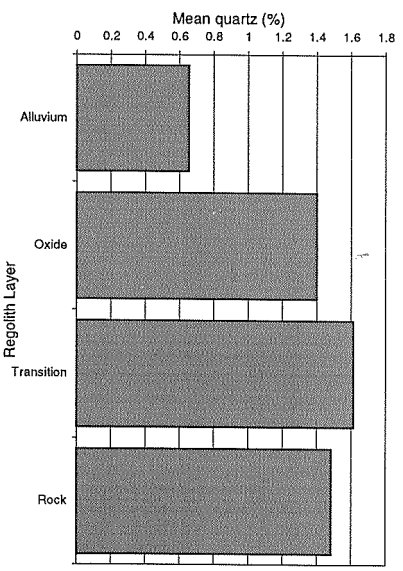

Figure 19: Mean quartz for each regolith layer from the Mt Joel 3000 mN prospect.

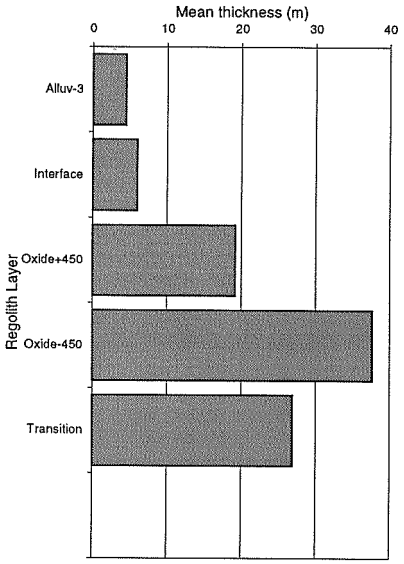

Figure 20: Mean thickness of regolith layers optimized for Au grade discrimination, from the Mt Joel 3000 mN prospect.

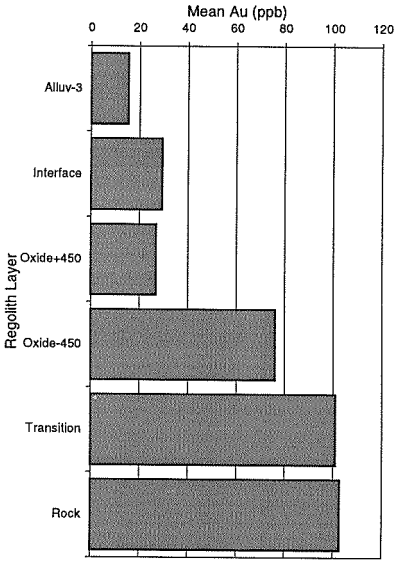

Figure 21: Mean Au for regolith layers optimized for Au grade discrimination, from the Mt Joel 3000 mN prospect.

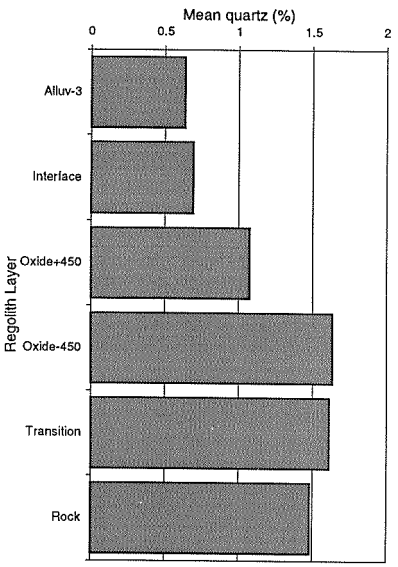

Figure 22: Mean quartz for regolith layers optimized for Au grade discrimination, from the Mt Joel 3000 mN prospect.

Further calculations of mean Au for the 3000 mN prospect are based on 3 m thick slices above and below the weathering front, the base of complete oxidation and the unconformity. The reliability of the results has been calculated using the method described in Section 2. Only those slices considered 60% reliable or greater were used. See Section 2 for clarification of these concepts.

Gold concentration, when calculated as a function of distance from the weathering front, is reasonably homogeneous above and below the front (Figure 23), although vein quartz shows a small increase above the weathering front (Figure 24). In contrast, Au content does vary when plotted as a function of distance from the BOCO (Figure 25). However, this may be due to variability in primary Au abundance, as suggested by the similar trend for quartz content (Figure 26). The lower Au content more than 20 m above the BOCO is consistent with the Au-poor upper oxide (Figure 21). This distinction between upper and lower oxide is more clearly observed for the calculations based on the unconformity (Figure 27). Note the depletion front approximately 24 m below the unconformity. The reduction in quartz content (Figure 28) is broader although still correlated with the Au trend.

As the regolith boundaries are horizontal or near-horizontal at the 3000 mN prospect, most of the features discussed above are visible in a plot of Au concentration vs. elevation (Figure 29). By restricting data to reliabilities of 60% or better, at each elevation Au concentrations for each regolith unit closely match the values for the entire *in situ* profile. Without this filtering, there are major discrepancies where the reliabilities for the data for individual units are less than 60%. Contents of both Au and quartz are lower above 450 mRL. As weathering in the saprolite is unlikely to cause quartz depletion, these lower abindances are probably primary.

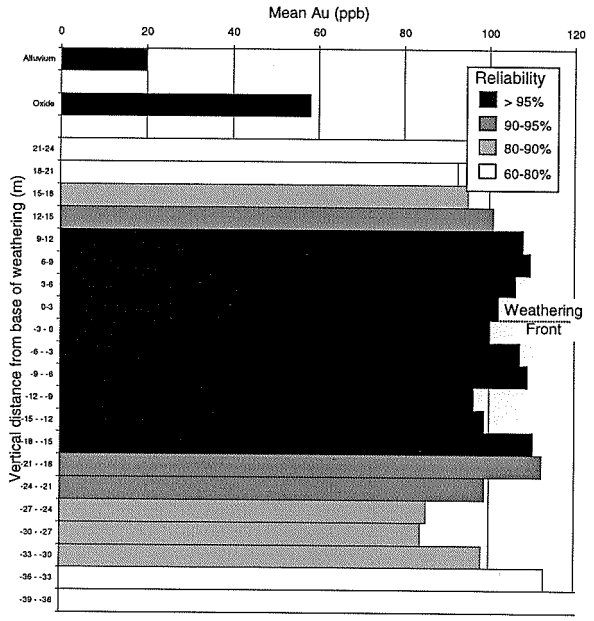

Figure 23: Mean Au vs. distance from the weathering front for the Mt Joel 3000 mN prospect.

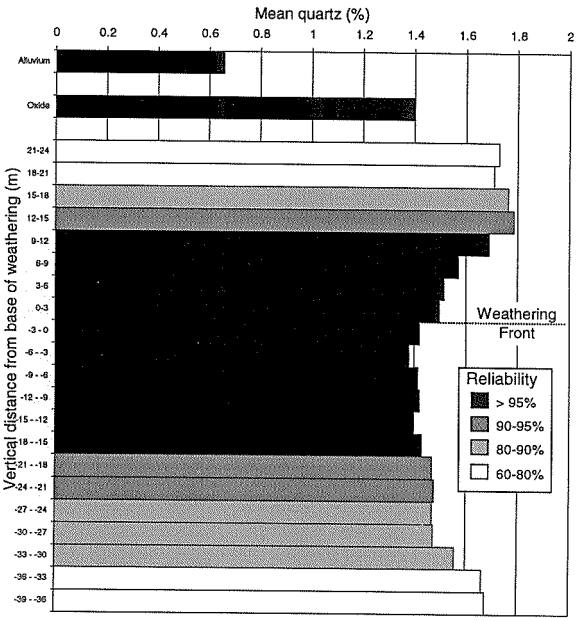

Figure 24: Mean quartz vs. distance from the weathering front for the Mt Joel 3000 mN prospect.

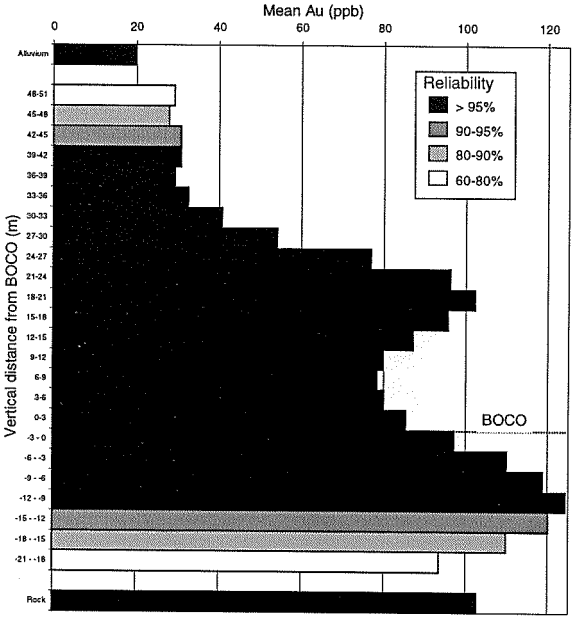

Figure 25: Mean Au vs. distance from the base of complete oxidation for the Mt Joel 3000 mN prospect.

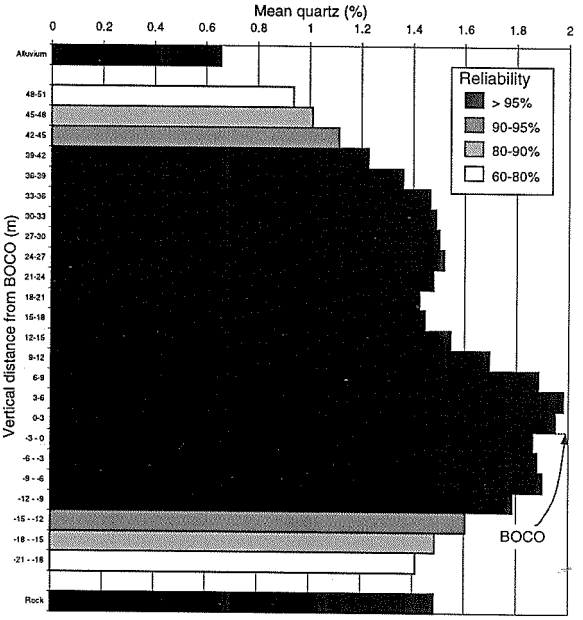

Figure 26: Mean quartz vs. distance from the base of complete oxidation for the Mt Joel 3000 mN prospect.

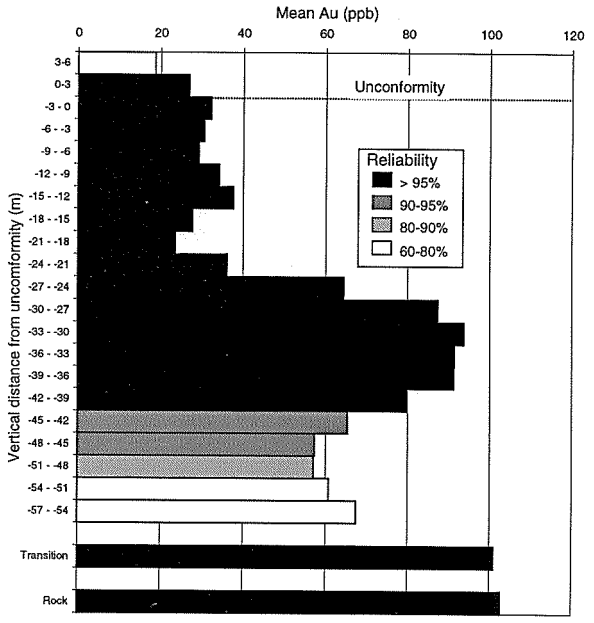

Figure 27: Mean Au vs. distance from the unconformity for the Mt Joel 3000 mN prospect.

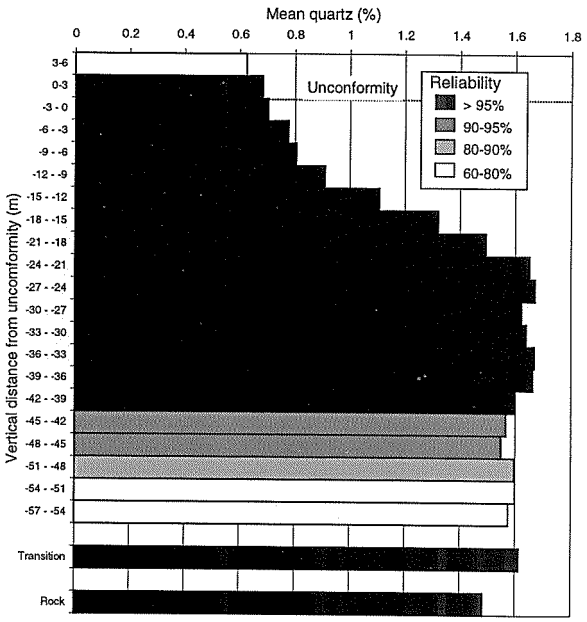

Figure 28: Mean quartz vs. distance from the unconformity for the Mt Joel 3000 mN prospect.

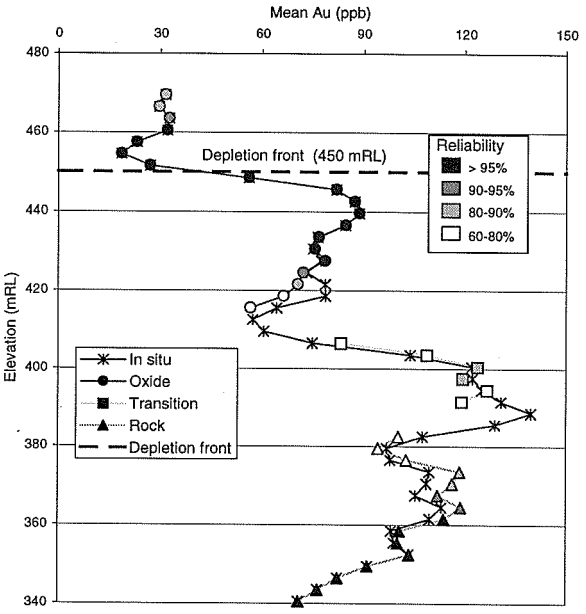

Figure 29: Mean Au vs. elevation for in situ regolith and rock at the Mt Joel 3000 mN prospect.

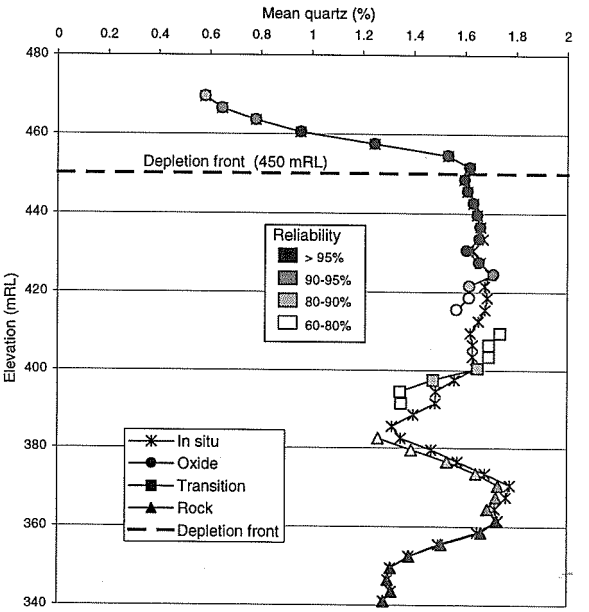

Figure 30: Mean quartz vs. elevation for in situ regolith and rock at the Mt Joel 3000 mN prospect.

Figure 31 (a) and (b) shows 50 and 100 ppb Au cut-off diagrams for the 3000 mN prospect. The Au anomaly at the interface between oxide and transported overburden is observed at a 50 ppb cut-off but is no longer visible when the cut-off is increased to 100 ppb. Vein quartz distribution (Figure 31 (c) and (c)) resembles that of Au, in terms of the diffuse nature of the mineralization, and lower contents at depth. However, quartz shows no "interface anomaly".

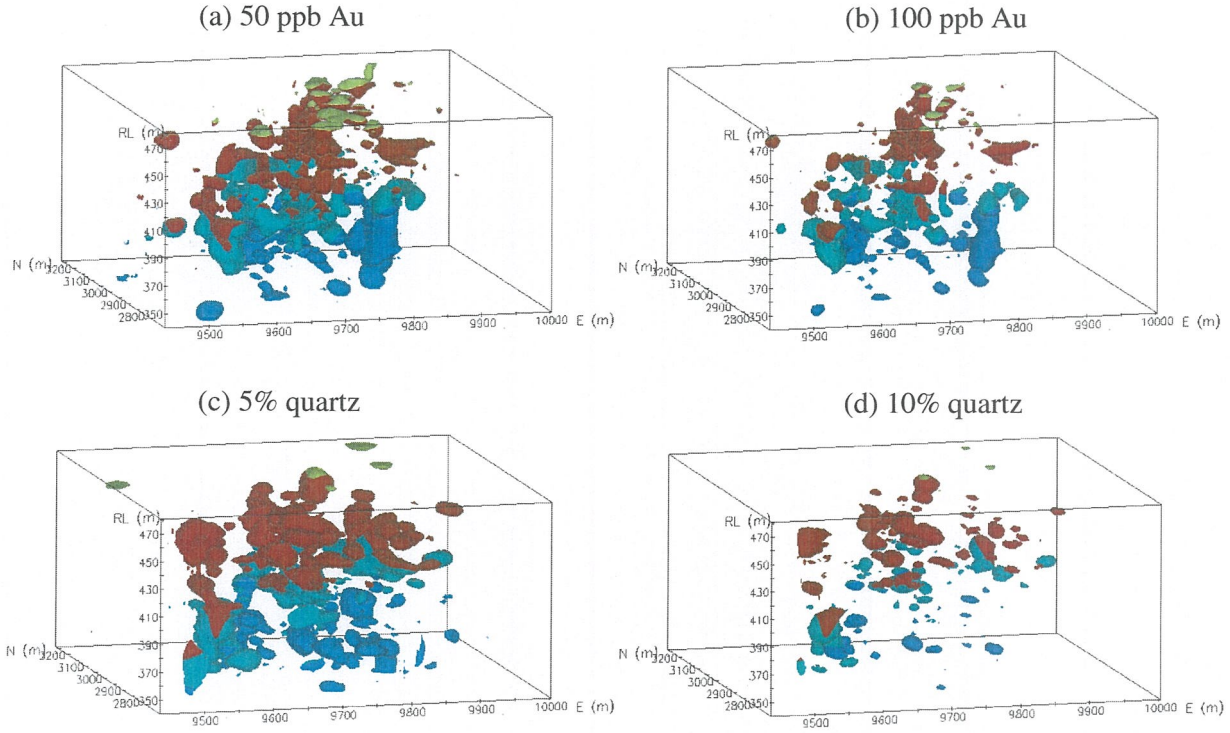

Figure 31: Gold distribution using (a) 50 ppb and (b) 100 ppb, and quartz distribution using (c) 5% and (d) 10% cut-offs for the 3000 mN prospect, Mt Joel, using a 2 x vertical exaggeration. Where Au or quartz are greater than the cut-off, the material is coloured according to the regolith horizon: blue - rock, green - transition, red - oxide, yellow - transported cover.

5.3 2400 mN prospect

At the 2400 mN prospect, the thicknesses of each regolith unit (alluvium – 10.4 m; oxide – 57 m; transition – 24.4 m; Figure 32) are almost identical to the 3000 mN prospect (Section 5.2) . Unlike the 3000 mN prospect, there is more Au in the transition (58 ppb), compared with the underlying rock (38 ppb) (Figure 33). The very similar pattern for quartz (Figure 34) suggests that this reflects primary Au content. There is a higher Au concentration in the oxide (65 ppb), but as expected, the transported cover is Au-poor (35 ppb). As at 3000 mN, the 3 m above and below the unconformity were combined into the interface. Also, the oxide (less the top 3 m) split into > 432 mRL and < 432 mRL (Figure 35), so as to emphasize the differences between the upper and lower portion of this unit (Figure 36). This new division of regolith zones indicates a Au-poor transported zone (27 ppb) (although almost twice the Au content of the alluvium at the 3000 mN prospect), over an enriched interface (59 ppb). The underlying oxide has a leached upper section (47 ppb Au), compared to the lower oxide (114 ppb Au). Note the lowering of the base of the Au-poor part of the oxide, from 450 mRL in the 3000 mN prospect to 432 mRL in the 2400 mN prospect. Results for quartz (Figure 37) show similar patterns, except that the interface is quartz poor, possibly due to destruction during weathering.

Further calculations of mean Au for the 2400 mN prospect are based on 3 m thick slices taken above and below the weathering front, the base of complete oxidation and the unconformity, with only those slices considered 60% reliable or greater used (Section 2).

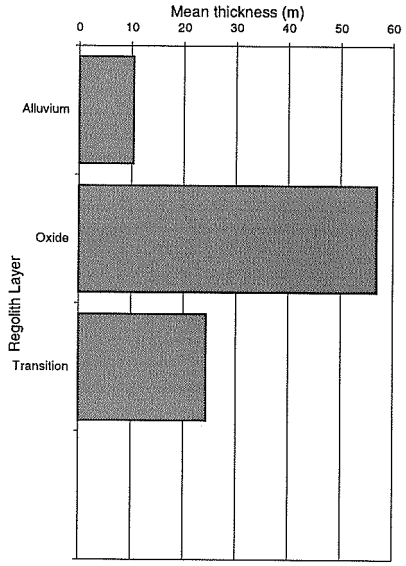

Figure 32: Mean thickness of each regolith layer from the Mt Joel 2400 mN prospect.

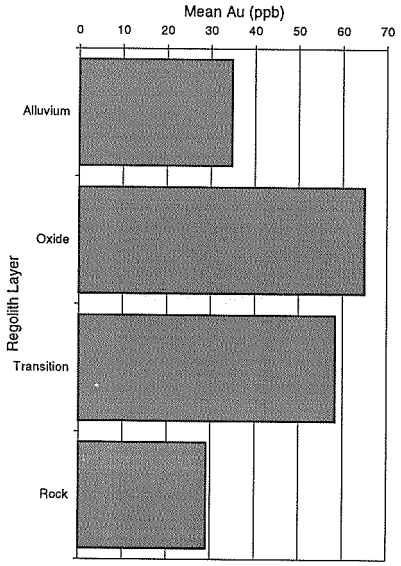

Figure 33: Mean Au for each regolith layer from the Mt Joel 2400 mN prospect.

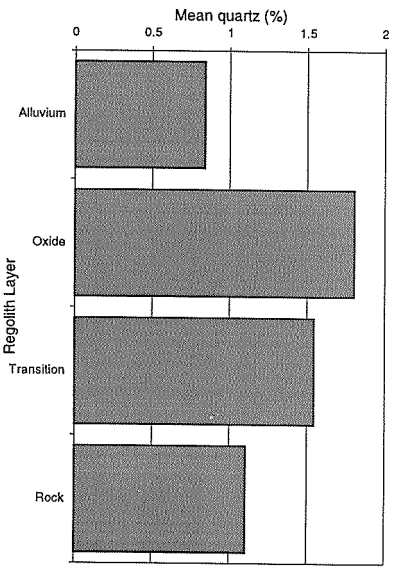

Figure 34: Mean quartz for each regolith layer from the Mt Joel 2400 mN prospect.

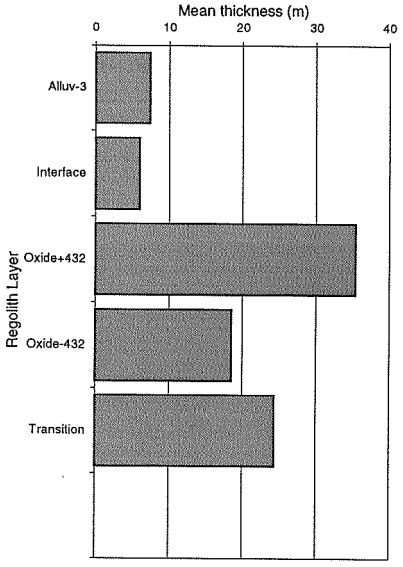

Figure 35: Mean thickness of regolith layers optimized for Au grade discrimination, from the Mt Joel 2400 mN prospect.

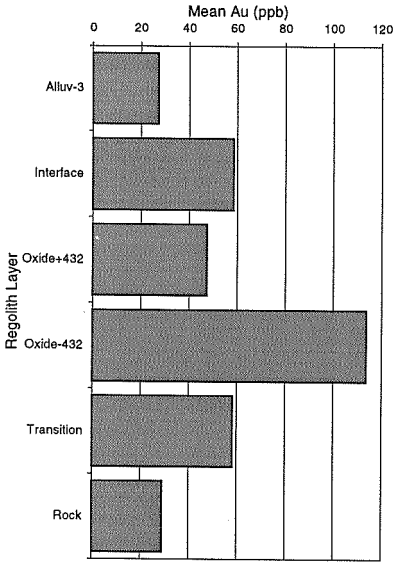

Figure 36: Mean Au for regolith layers optimized for Au grade discrimination, from the Mt Joel 2400 mN prospect.

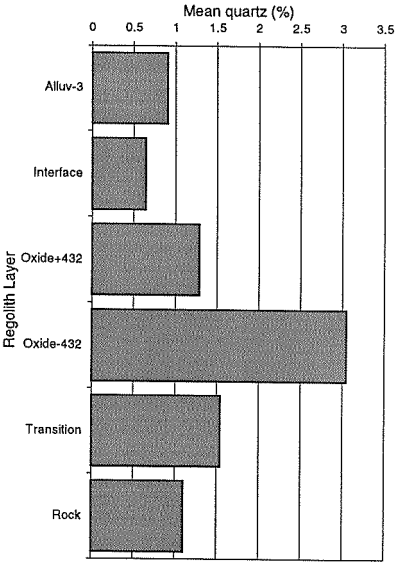

Figure 37: Mean quartz for regolith layers optimized for Au grade discrimination, from the Mt Joel 2400 mN prospect.

There are no consistent variations in Au (Figure 38) or quartz (Figure 39) concentration about the weathering front. Unlike 3000 mN, Au concentrations increase up through the base of complete oxidation (Figure 40). The different results for the two prospects possibly merely reflect grade variations prior to weathering. In contrast, the lower Au content in the upper oxide (at greater than 40 m above the base of complete oxidation; Figure 40) is a proportionally greater change, consistent with results for the 3000 mN prospect (Section 5.2), although it again correlates with a zone of low quartz (Figure 41). This distinction between upper and lower oxide is clearer for calculations based on the unconformity surface (Figure 42), with the Au-poor zone going deeper than for the 3000 mN prospect (Figure 27). Quartz is also lowered close to the interface (Figure 43).

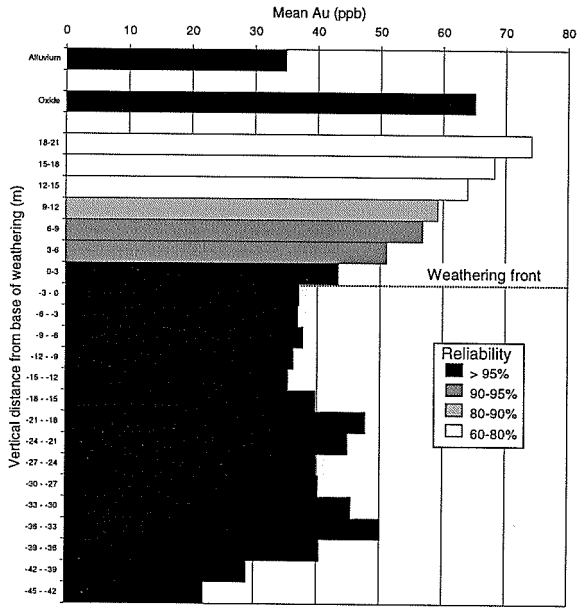

Figure 38: Mean Au vs. distance from the weathering front for the Mt Joel 2400 mN prospect.

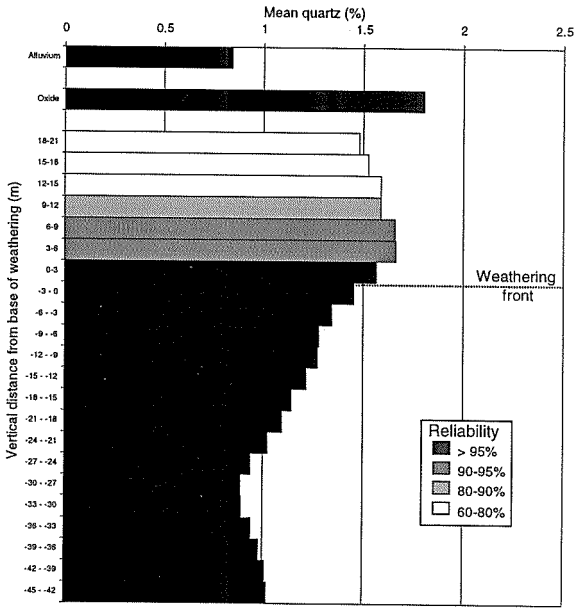

Figure 39: Mean quartz vs. distance from the weathering front for the Mt Joel 2400 mN prospect.

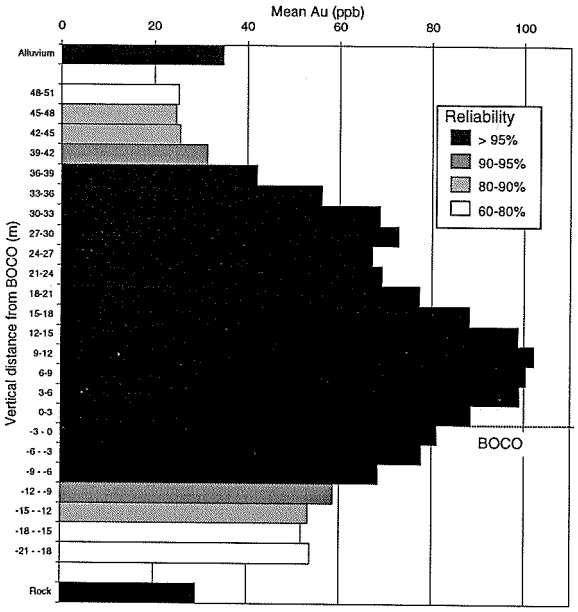

Figure 40: Mean Au vs. distance from the base of complete oxidation for the Mt Joel 2400 mN prospect.

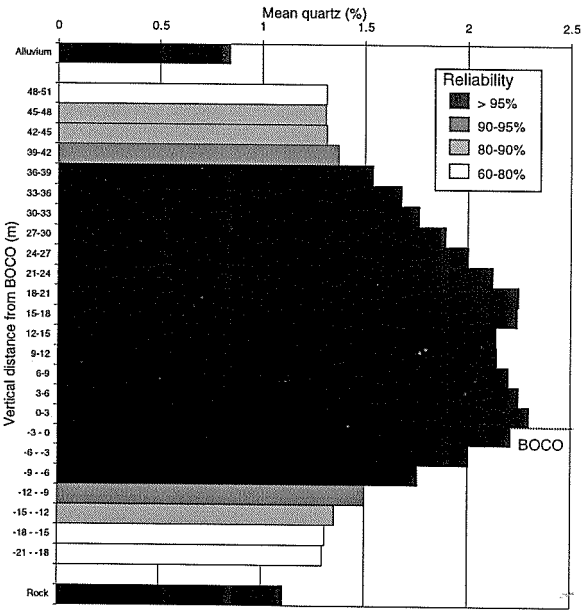

Figure 41: Mean quartz vs. distance from the base of complete oxidation for the Mt Joel 2400 mN prospect.

This Au-poor zone (with the base estimated at 432 mRL) is clearly observed for the Au vs. elevation plot (Figure 44), with a marked peak in Au content approximately 8 m below the depletion front. The very similar pattern for quartz (Figure 45), suggests the bulk of this variation to be primary.

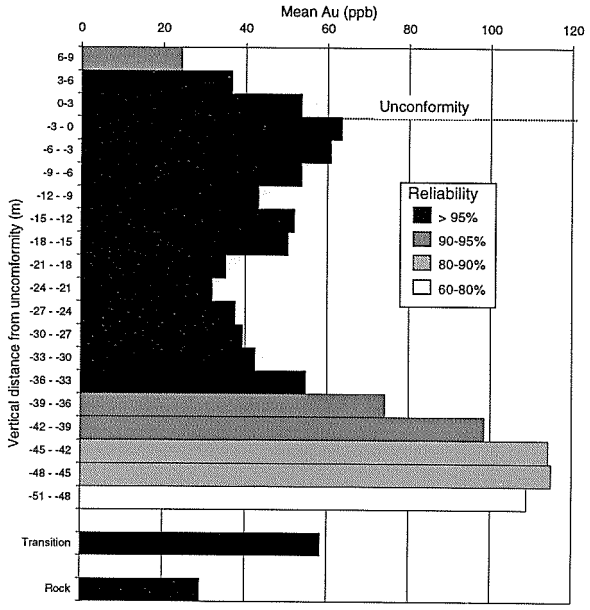

Figure 42: Mean Au vs. distance from the unconformity for the Mt Joel 2400 mN prospect.

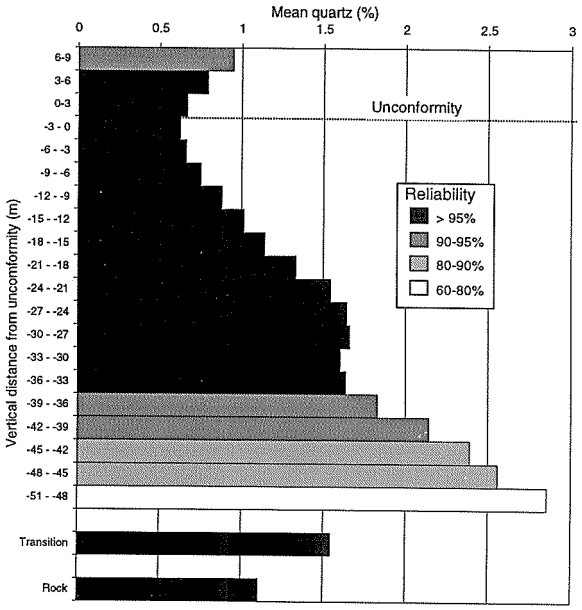

Figure 43: Mean quartz vs. distance from the unconformity for the Mt Joel 2400 mN prospect.

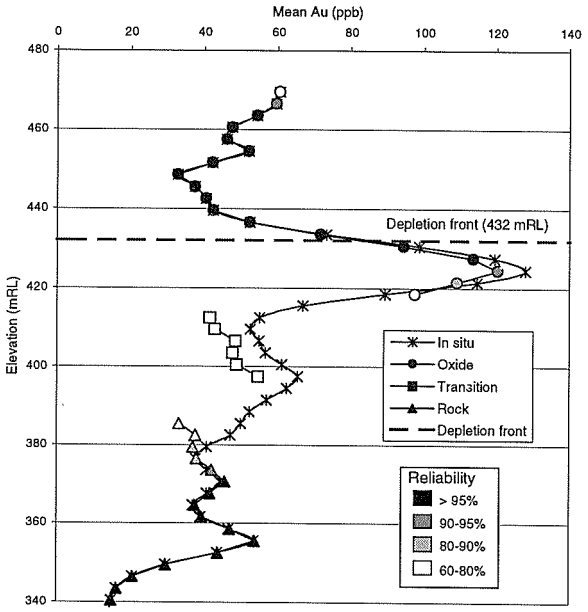

Figure 44: Mean Au vs. elevation for residuum and rock at the Mt Joel 2400 mN prospect.

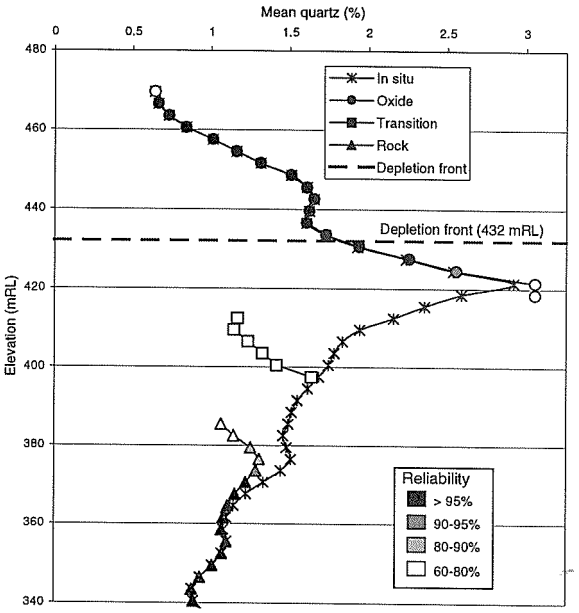

Figure 45: Mean quartz vs. elevation for residuum and rock at the Mt Joel 2400 mN prospect.

Figure 46 shows 50 and 100 ppb Au and 5 and 10% quartz cut-off diagrams for the 2400 mN prospect. In a similar manner to the 3000 mN prospect, the Au interface anomaly is clearly observed at a 50 ppb cut-off, whereas quartz concentration is low at the interface. Both Au and quartz contents are generally low (Au < 50 ppb, quartz < 5%) more than 10 m below the weathering front.

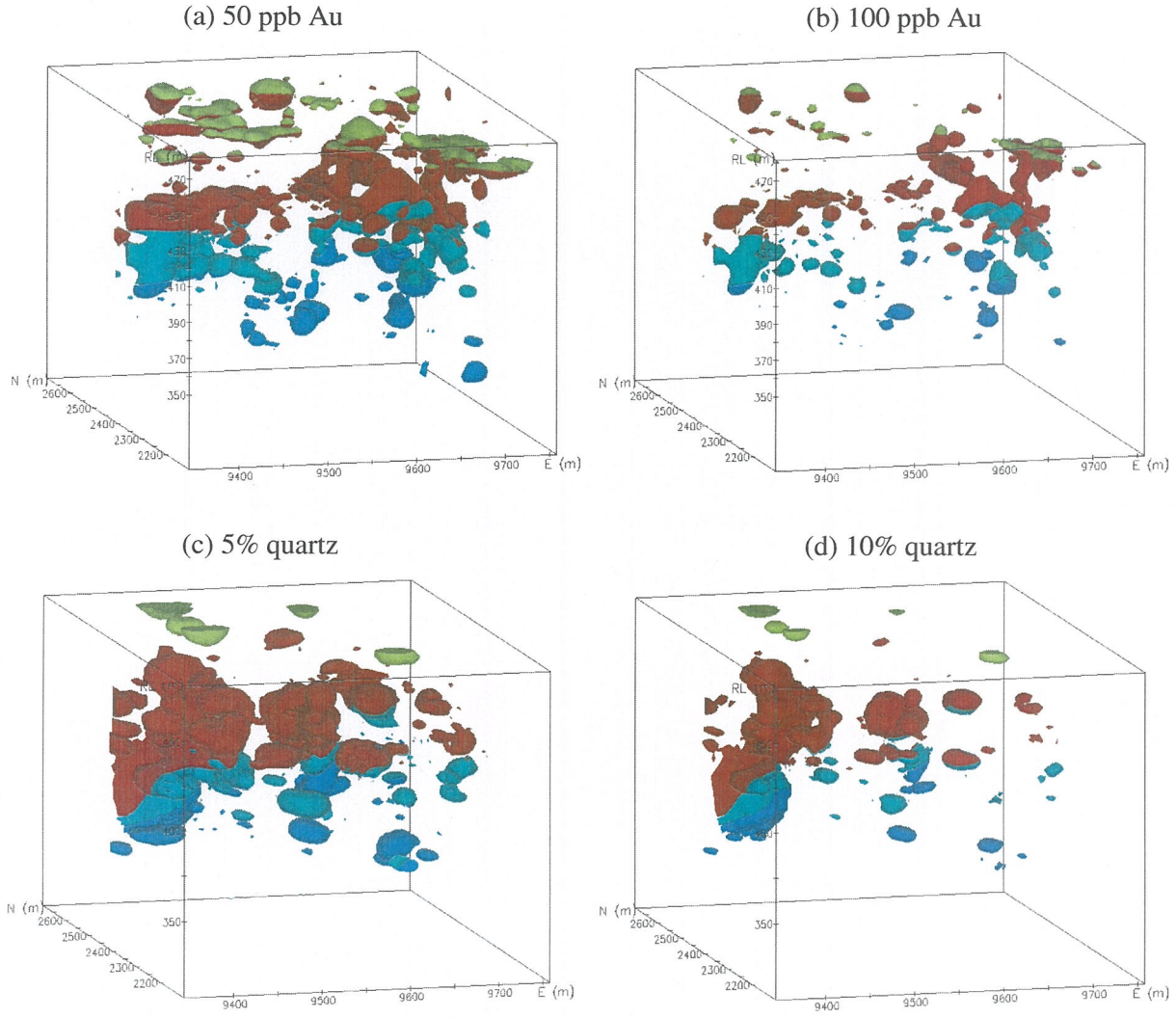

Figure 46: Gold distribution using (a) 50 ppb and (b) 100 ppb, and quartz distribution using (c) 5% and (d) 10% cut-offs for the 2400 mN prospect, Mt Joel, using a 2 x vertical exaggeration. Where Au or quartz are greater than the cut-off, the material is coloured according to the regolith horizon: blue - rock, green - transition, red - oxide, yellow - transported cover.

5.4 1600 mN prospect

There is a much greater thickness of transported cover (60.3 m) at the 1600 mN prospect (Figure 47) than to the north. Within the *in situ* regolith, the oxide and transition horizons have similar thicknesses (26.5 and 30.7 m, respectively). This contrasts with the 3000 and 2400 mN prospects (Sections 5.2 and 5.3) at which the oxide is dominant and more than twice as thick. There is significantly less Au (Figure 48) in the oxide (77 ppb) than the underlying transition (133 ppb). The transported cover is Au-poor (18 ppb) as well as having significantly less quartz than the residuum (Figure 49). When slices 3 m above and below the unconformity are combined into the interface (Figure 50), there is no enrichment (44 ppb Au) relative to the underlying upper oxide (53 ppb Au) (Figure 51). The upper oxide at the 1600 mN prospect has been defined as a thin layer > 414 mRL (Figure 20). This small thickness of upper oxide (Figure 50) provides a less distinct depletion than at the 3000 and 2400 mN prospects (Sections 5.2 and 5.3). However, the lowering of the depletion front, relative to the 3000 and 2400 mN sites, is consistent with the previous results and, like the 3000 and 2400 mN prospects, the quartz data also show a similar pattern (Figure 52).

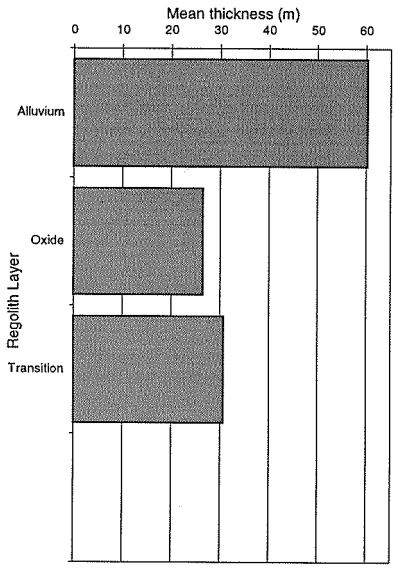

Figure 47: Mean thickness of each regolith layer from the Mt Joel 1600 mN prospect.

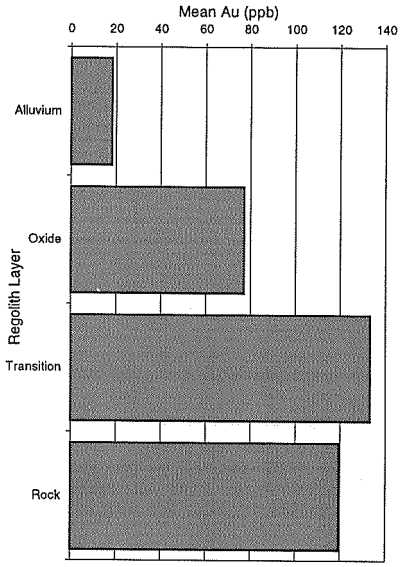

Figure 48: Mean Au for each regolith layer from the Mt Joel 1600 mN prospect.

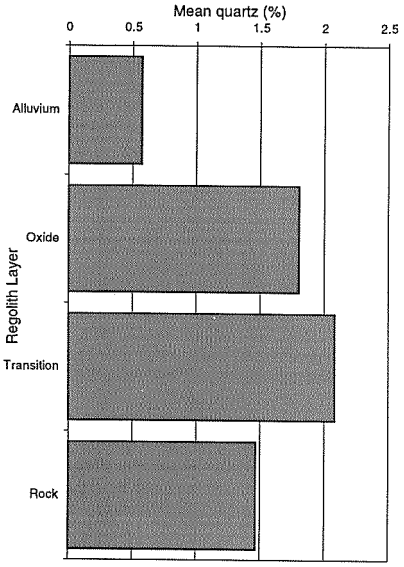

Figure 49: Mean quartz for each regolith layer from the Mt Joel 1600 mN prospect.

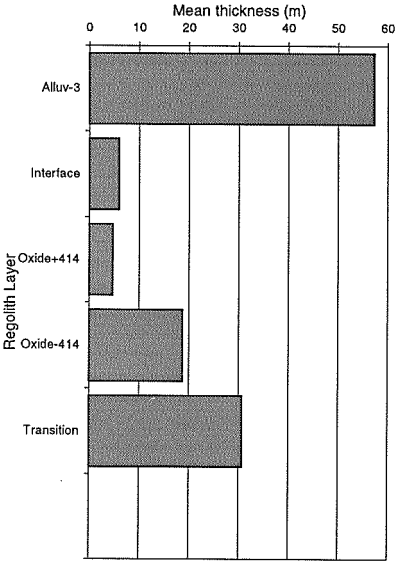

Figure 50: Mean thickness of regolith layers optimized for Au grade discrimination, from the Mt Joel 1600 mN prospect.

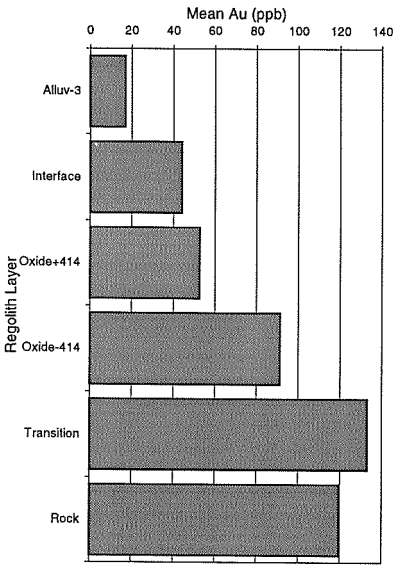

Figure 51: Mean Au for regolith layers optimized for Au grade discrimination, from the Mt Joel 1600 mN prospect.

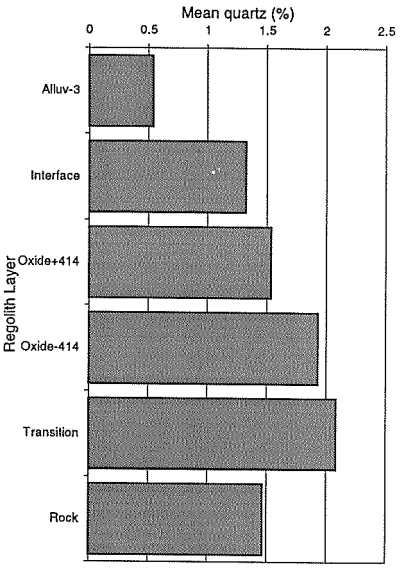

Figure 52: Mean quartz for regolith layers optimized for Au grade discrimination, from the Mt Joel 1600 mN prospect.

Calculations of mean Au content as a function of distance from the weathering front (Figure 53) show lower Au concentrations directly above the weathering front, which differs from the other sites. The pattern for quartz content about the weathering front is significantly different (Figure 54). In contrast, across the base of complete oxidation, there is little variation in Au concentration (Figure 55) and virtually none for quartz (Figure 56). As discussed above, the lower Au content 12 m above the BOCO is consistent with a Au-poor zone in the upper oxide. This distinction between upper and lower oxide is more clearly observed in the graph depicting mean Au based on the unconformity, at approximately 12 m below this boundary (Figure 57). This graph also clearly demonstrates the enrichment at the interface .

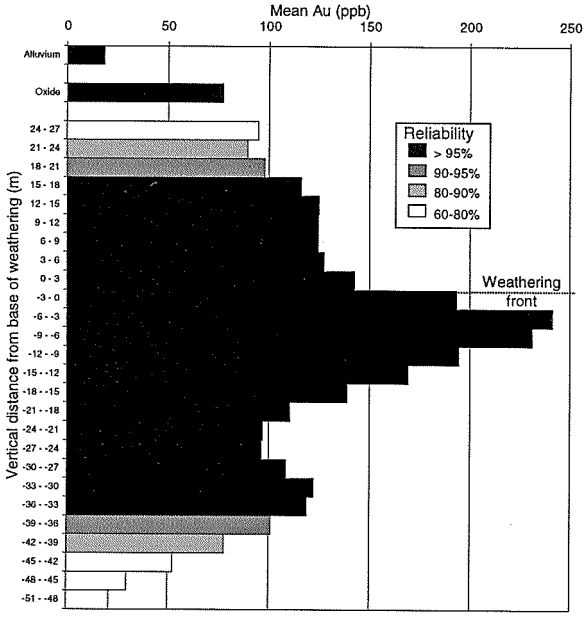

Figure 53: Mean Au vs. distance from the weathering front for the Mt Joel 1600 mN prospect.

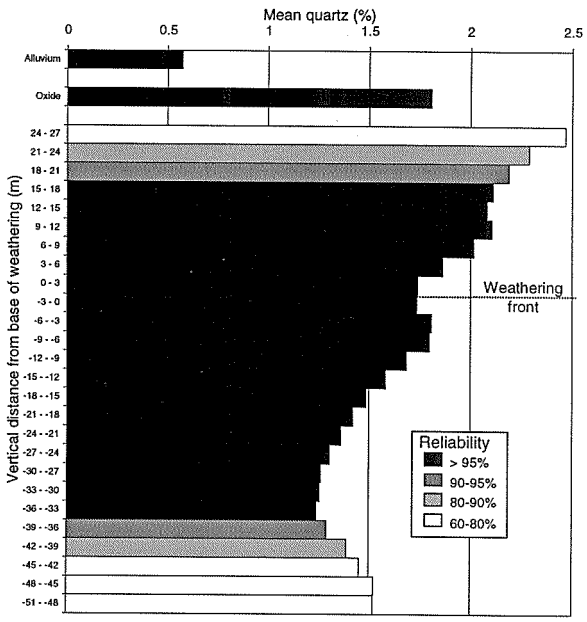

Figure 54: Mean quartz vs. distance from the weathering front for the Mt Joel 1600 mN prospect.

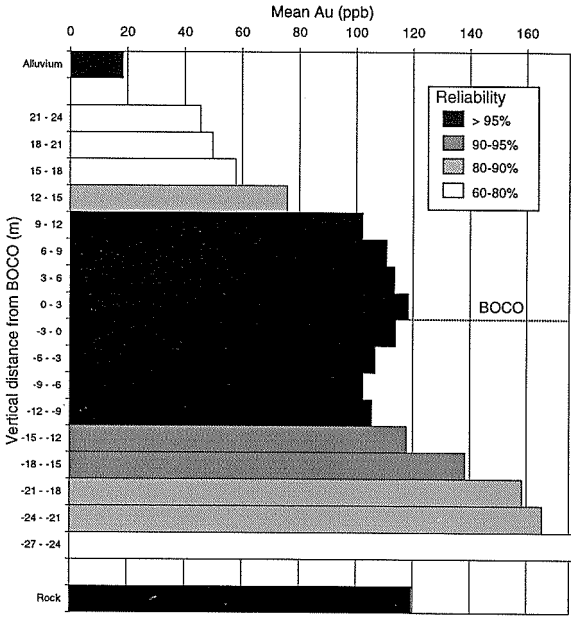

Figure 55: Mean Au vs. distance from the base of complete oxidation for the Mt Joel 1600 mN prospect.

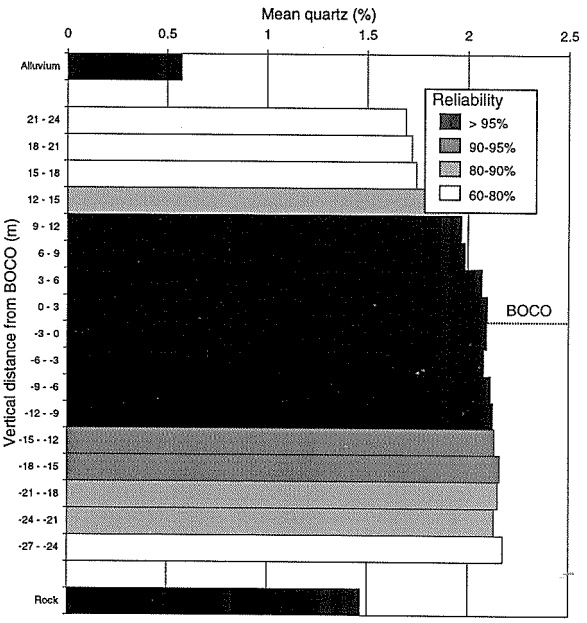

Figure 56: Mean quartz vs. distance from the base of complete oxidation for the Mt Joel 1600 mN prospect.

As the regolith boundaries are horizontal or near-horizontal at the 1600 mN prospect, most of the features already discussed are visible in a plot of Au concentration vs. elevation (Figure 59). By restricting data to reliabilities of 60% or better, Au concentrations for each regolith unit closely match the values for the entire *in situ* profile. Most of the variation in Au concentration in the *in situ* regolith is of a similar order to the variation in the bedrock. The exception is the upper oxide zone, which has significantly less Au than below. However, the thinness of this zone makes the existence

of this zone less convincing than for the 3000 and 2400 mN prospects. Some of the features for Au variation vs. depth in the *in situ* profile are also observed for quartz (Figure 60), most notably the low at approximately 330 mRL and the thin depleted zone at the top of the residuum.

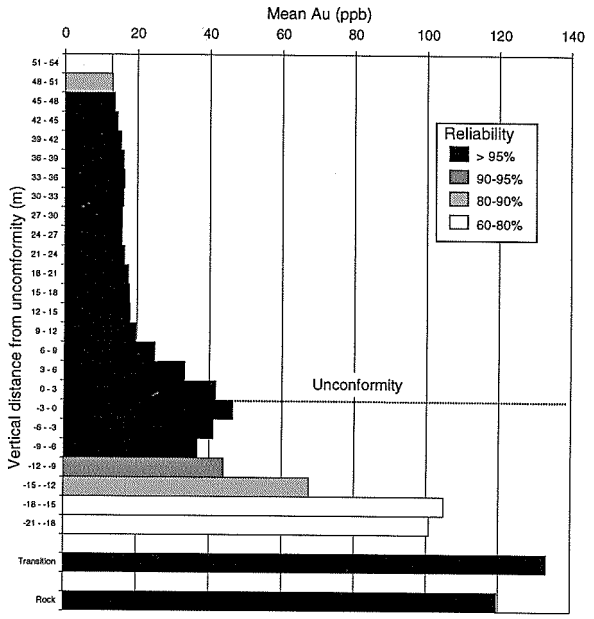

Figure 57: Mean Au vs. distance from the unconformity for the Mt Joel 1600 mN prospect.

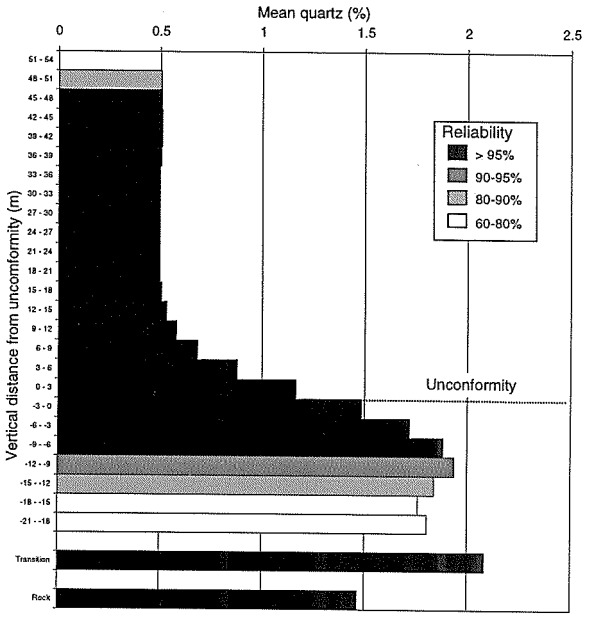

Figure 58: Mean quartz vs. distance from the unconformity for the Mt Joel 1600 mN prospect.

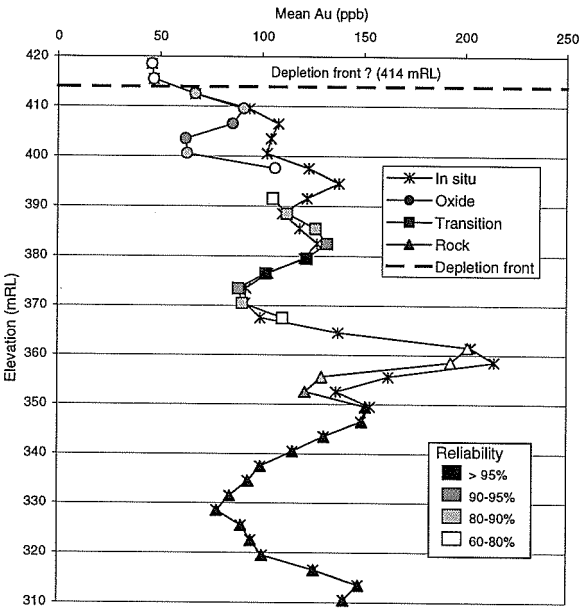

Figure 59: Mean Au vs. elevation for in situ regolith and rock at the Mt Joel 1600 mN prospect.

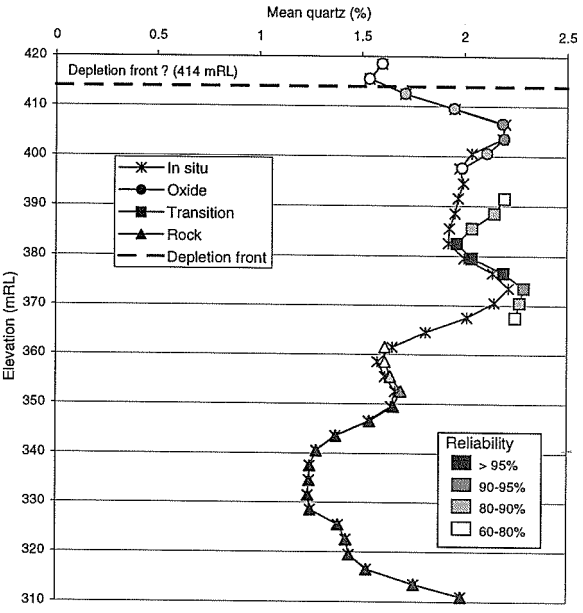

Figure 60: Mean quartz vs. elevation for in situ regolith and rock at the Mt Joel 1600 mN prospect.

The mineralization at 1600 mN differs from that further north in that the Au distribution appears more closely controlled by major structural factors (Figure 61 (a) and (b)), primarily running N-S. These features are also observed for the quartz vein distribution (Figure 61 (c) and (d)).

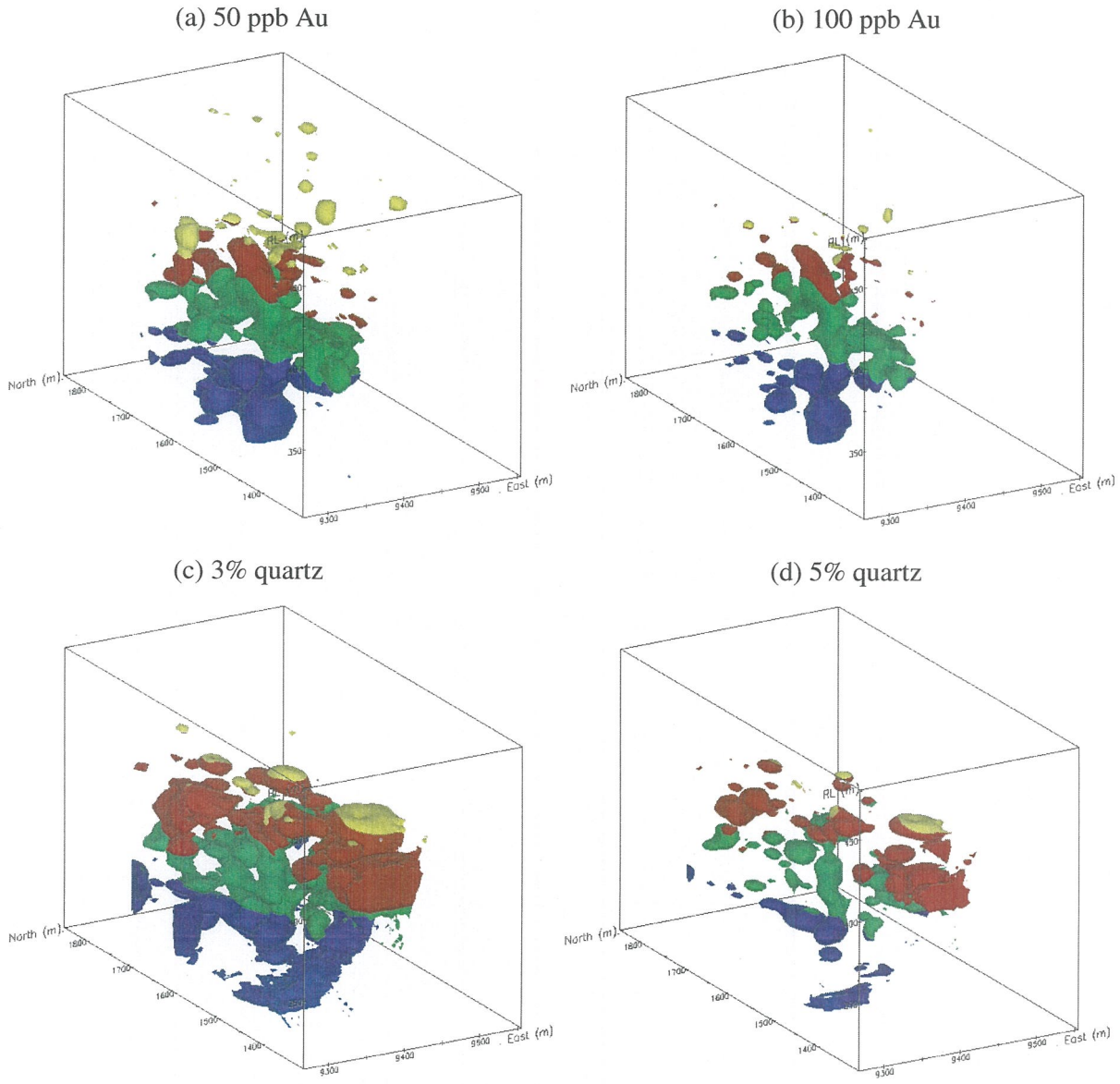

Figure 61: Gold distribution using (a) 50 ppb and (b) 100 ppb, and quartz distribution using (c) 3% and (d) 5% cut-offs for the 1600 mN prospect, Mt Joel, using a 2 x vertical exaggeration. Where Au or quartz are greater than the cut-off, the material is coloured according to the regolith horizon: blue - rock, green - transition, red - oxide, yellow - transported cover.

5.5 800 mN prospect

The thickness of transported cover (60.1 m) in the 800 mN prospect (Figure 62) is virtually identical to that in the 1600 mN prospect (Section 5.4). However, in the 800 mN prospect the oxide (33.9 m) is thicker than the transition (18.8 m), although it is still substantially thinner than at the 3000 and 2400 mN prospects (Sections 5.2 and 5.3). Mean Au concentrations (Figure 63) increase from rock (42 ppb) to the transition (57 ppb) and the oxide (76 ppb). A similar increase was observed for the 2400 mN prospect but not the 3000 and 1600 mN prospects. The transported cover is Au-poor (23 ppb). When the 3 m above and below the unconformity are combined into the interface (Figure 65), this shows a major enrichment (111 ppb Au), relative to the underlying oxide (72 ppb Au) (Figure 66). There is no evidence for a Au-poor zone within the oxide (see below). Unlike the other sites, there is a very poor correlation between the Au and quartz (Figure 67) content. It is not known why this prospect differs from the other four prospects, although it could relate to the style of the mineralization.

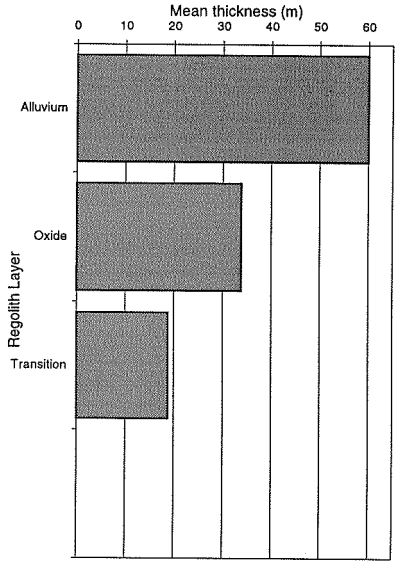

Figure 62: Mean thickness of each regolith layer from the Mt Joel 800 mN prospect.

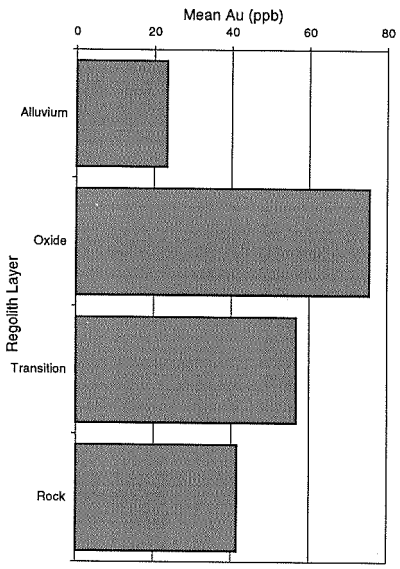

Figure 63: Mean Au for each regolith layer from the Mt Joel 800 mN prospect.

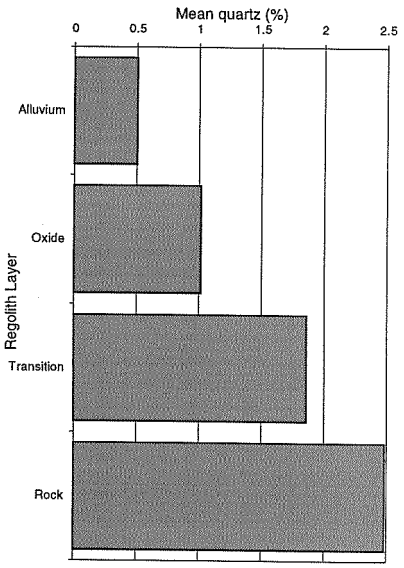

Figure 64: Mean quartz for each regolith layer from the Mt Joel 800 mN prospect.

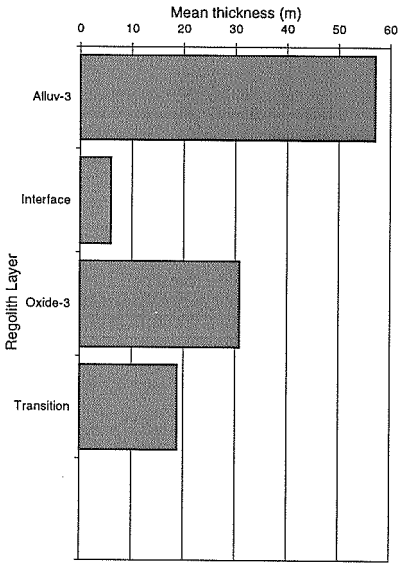

Figure 65: Mean thickness of regolith layers optimized for Au grade discrimination, from the Mt Joel 800 mN prospect.

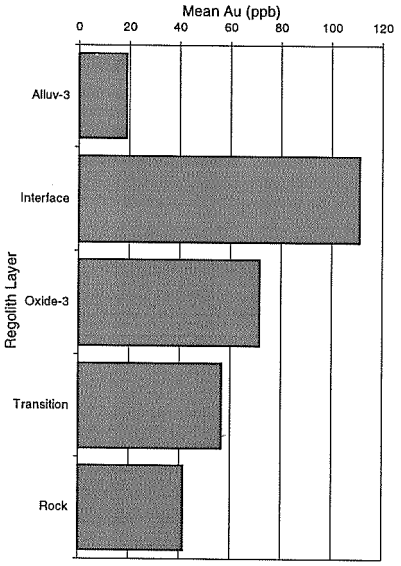

Figure 66: Mean Au for regolith layers optimized for Au grade discrimination, from the Mt Joel 800 mN prospect.

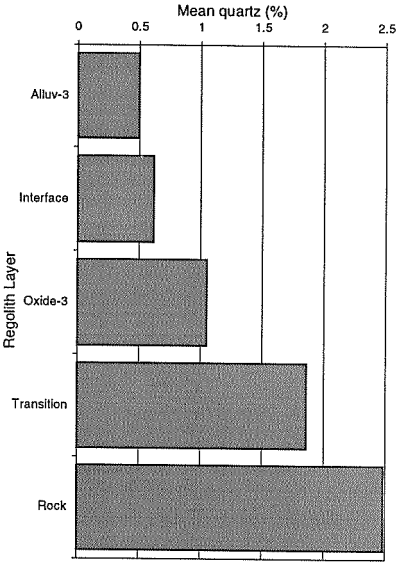

Figure 67: Mean quartz for regolith layers optimized for Au grade discrimination, from the Mt Joel 800 mN prospect.

Calculations of mean Au content as a function of distance from the weathering front (Figure 68) show higher Au concentrations directly above the front. High Au values also occur at the base of complete oxidation (Figure 70). Comparison with other sites suggest these variations to be dominantly primary. On the other hand, the interface enrichment is clearly observed (Figure 72), and is consistent with the other prospects (Sections 5.2 - 5.4). As discussed in Section 4.3, there was little improvement in the data contrast by gridding and analysing at higher resolution (Figure 74). The enrichment of Au at the unconformity is also observed in a plot of Au concentration vs. elevation (Figure 75).

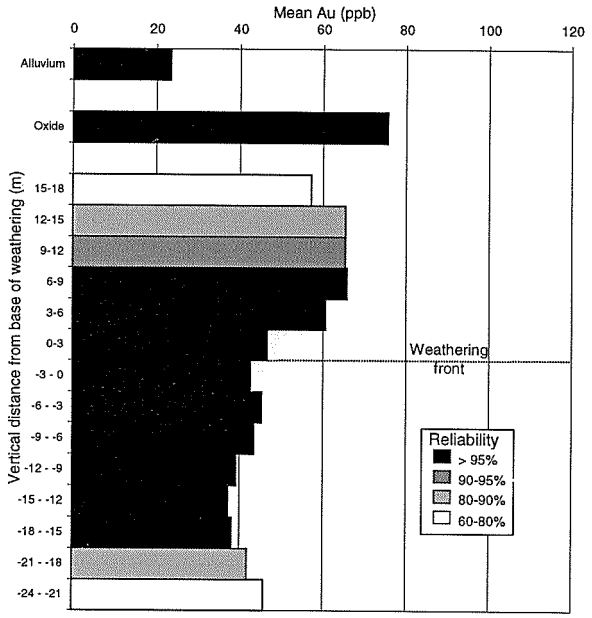

Figure 68: Mean Au vs. distance from the weathering front for the Mt Joel 800 mN prospect.

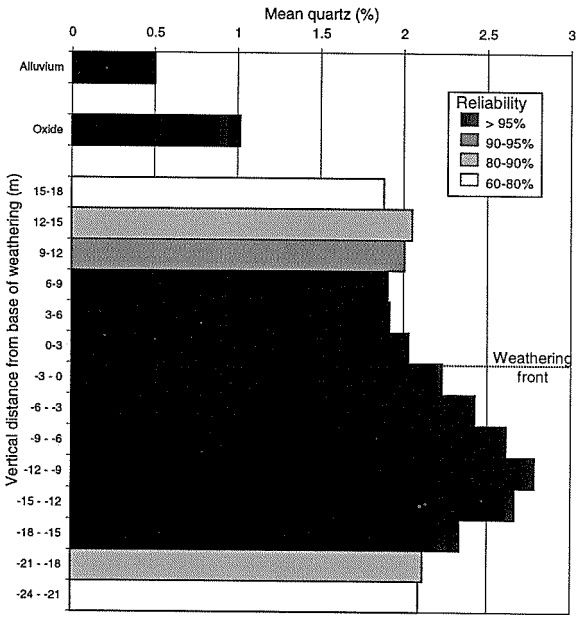

Figure 69: Mean Au vs. distance from the weathering front for the Mt Joel 800 mN prospect.

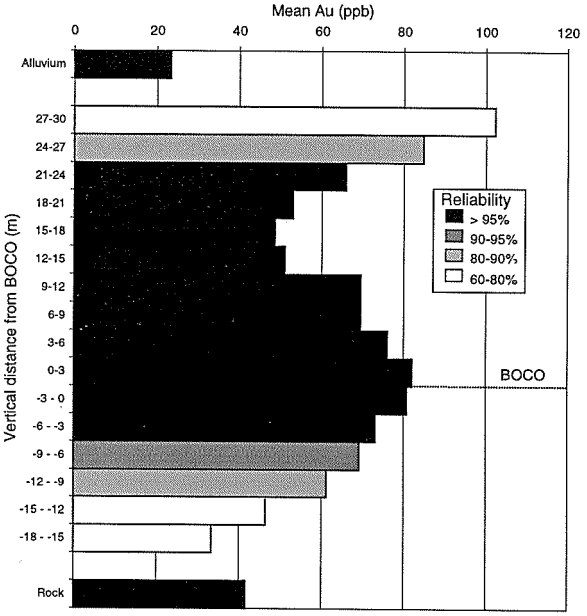

Figure 70: Mean Au vs. distance from the base of complete oxidation for the Mt Joel 800 mN prospect

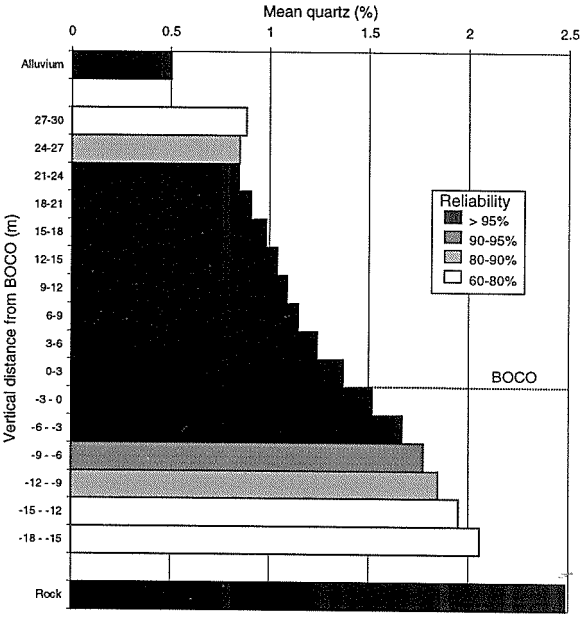

Figure 71: Mean quartz vs. distance from the base of complete oxidation for the Mt Joel 800 mN prospect

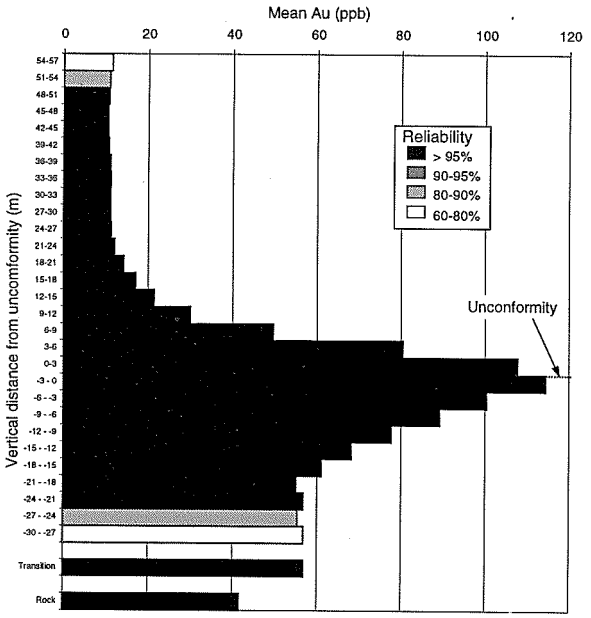

Figure 72: Mean Au vs. distance from the unconformity for the Mt Joel 800 mN prospect.

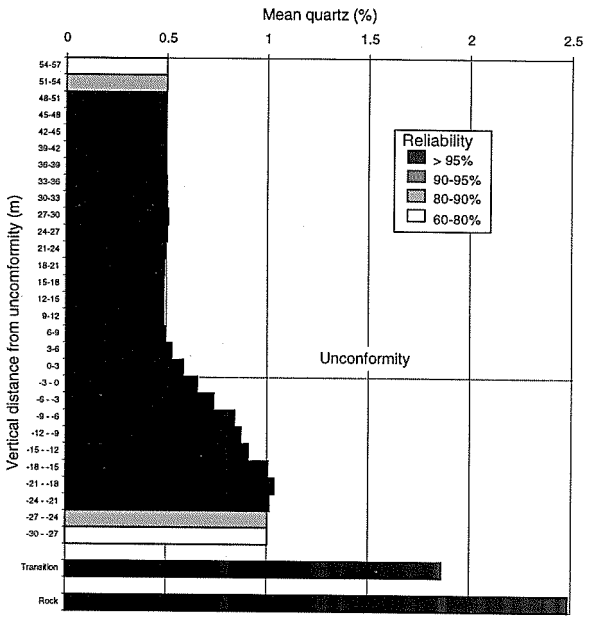

Figure 73: Mean quartz vs. distance from the unconformity for the Mt Joel 800 mN prospect.

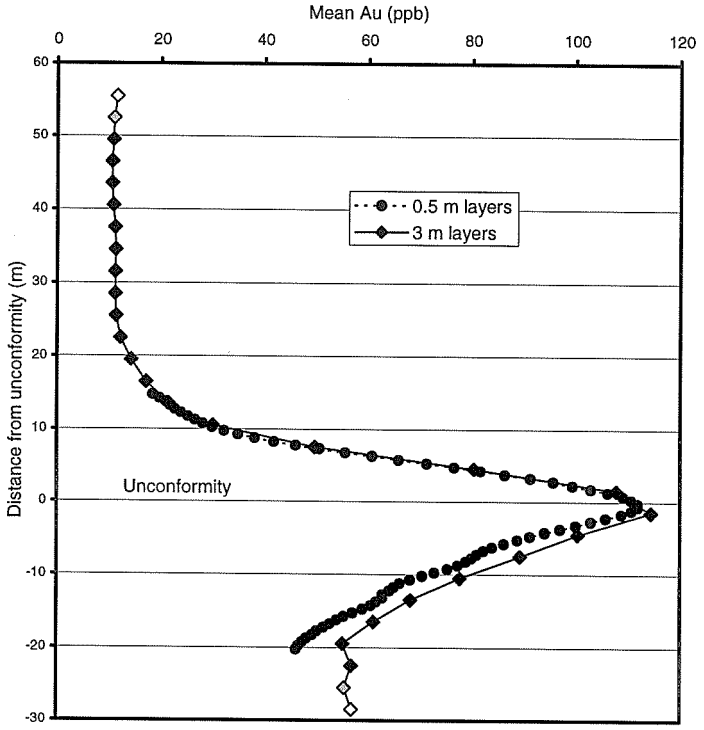

Figure 74: Mean Au vs. distance from the unconformity ("normal" and "fine" gridding) for the Mt Joel 800 mN prospect.

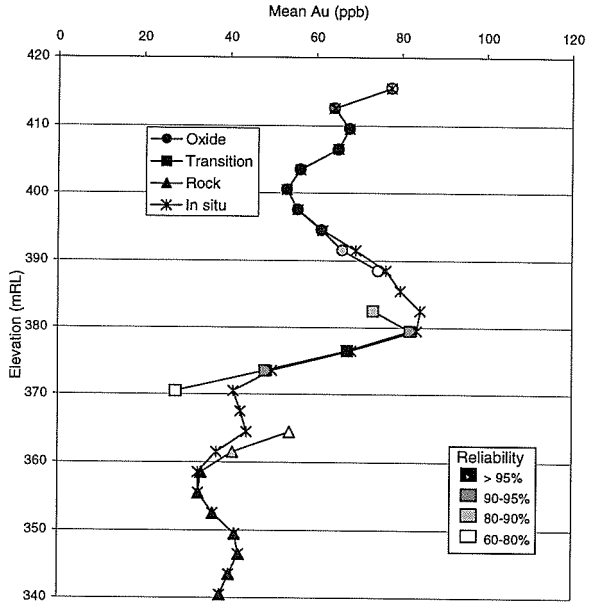

Figure 75: Mean Au vs. elevation for in situ regolith and rock at the Mt Joel 800 mN prospect.

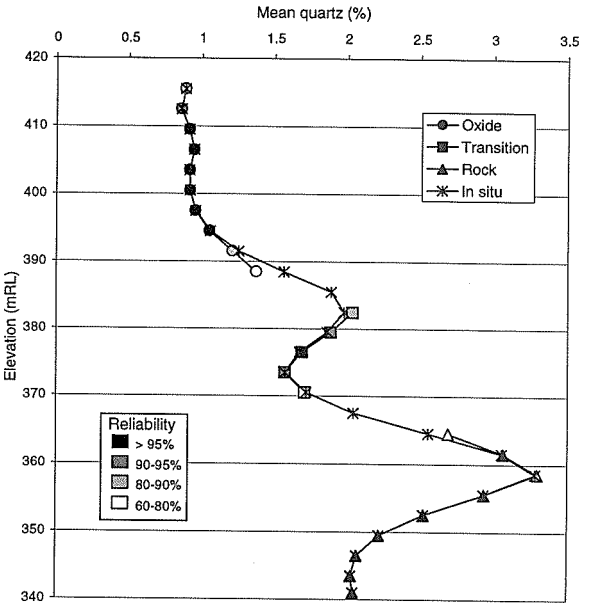

Figure 76: Mean quartz vs. elevation for in situ regolith and rock at the Mt Joel 800 mN prospect.

The interface enrichment in Au for the 800 mN prospect is clearly shown for the cut-off diagrams (Figure 77 (a) and (b)). Quartz distribution (Figure 77 (c) and (d)) less closely matches Au than at the other prospects.

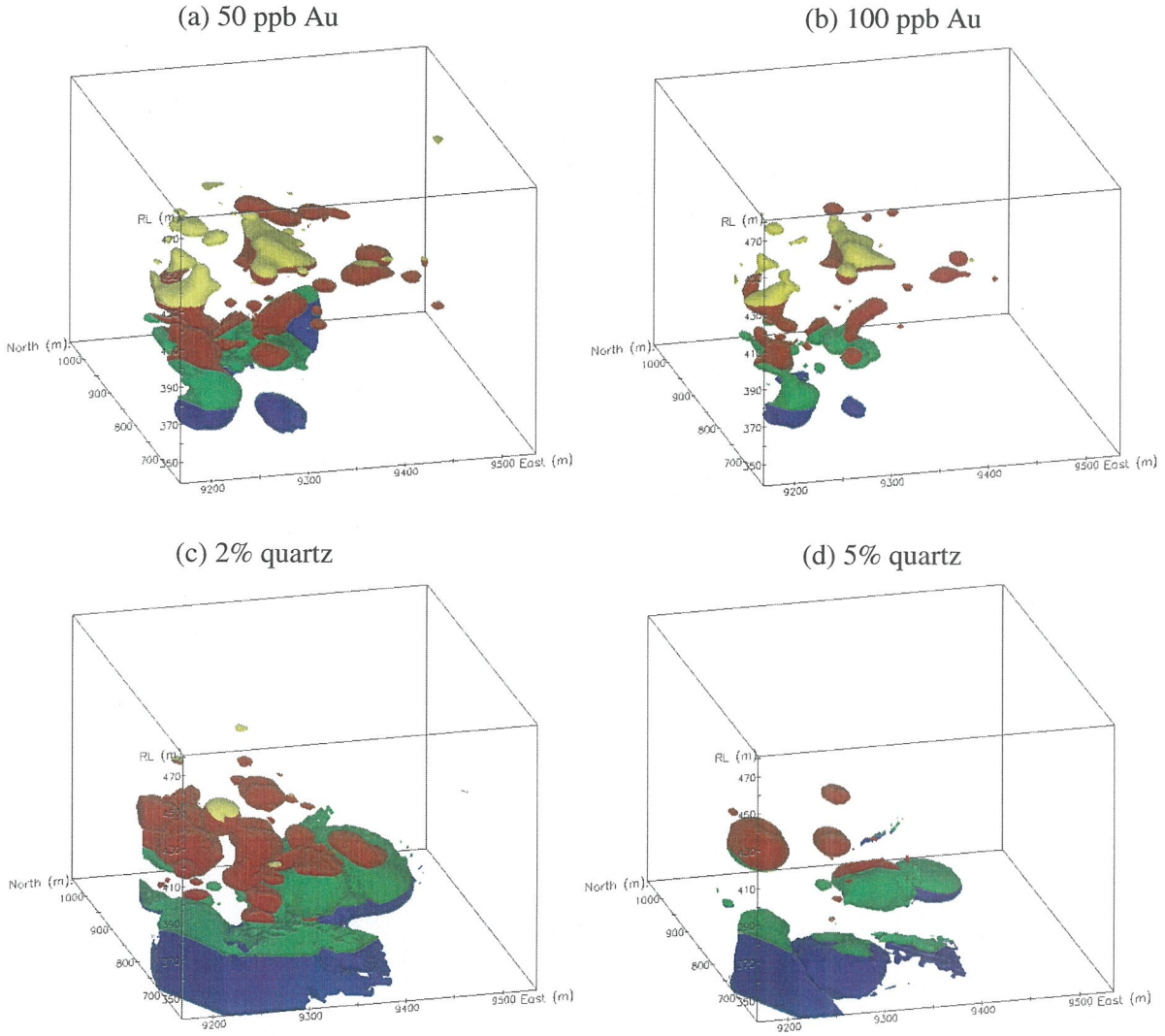

Figure 77: Gold distribution using (a) 50 ppb and (b) 100 ppb, and quartz distribution using (c) 2% and (d) 5% cut-offs for the 800 mN prospect, Mt Joel, using a 2 x vertical exaggeration. Where Au or quartz are greater than the cut-off, the material is coloured according to the regolith horizon: blue - rock, green - transition, red - oxide, yellow - transported cover.

5.6 0 mN prospect

The 0 mN prospect has thinner alluvium (20.5 m) and oxide (19.6 m) than the 800 mN prospect (Figure 78), but a thicker transition (25.8 m). Also in contrast with the 800 mN prospect, (Section 5.5), the Au concentration (Figure 79) is lower in the oxide (54 ppb) than in the transition (84 ppb). Indeed, as discussed in previous Sections, variation in mean Au concentration in bedrock, transition and oxide appears to be mainly a consequence of primary variation. The transported cover has lower Au content (38 ppb) than the *in situ* regolith, but it is relatively high compared with the other prospects (Sections 5.2 to 5.5). When the 3 m above and below the unconformity are combined into the interface (Figure 81), a major enrichment (78 ppb Au), relative to the underlying oxide (49 ppb Au) can be seen (Figure 82). There is no evidence for a depletion front within the oxide (see below). The quartz distribution (Figure 80 and Figure 83) appears similar to that of Au, but, as elsewhere, without the enrichment at the interface.

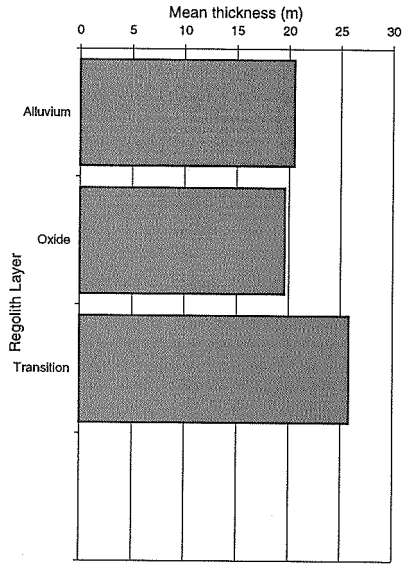

Figure 78: Mean thickness of each regolith layer from the Mt Joel 0 mN prospect.

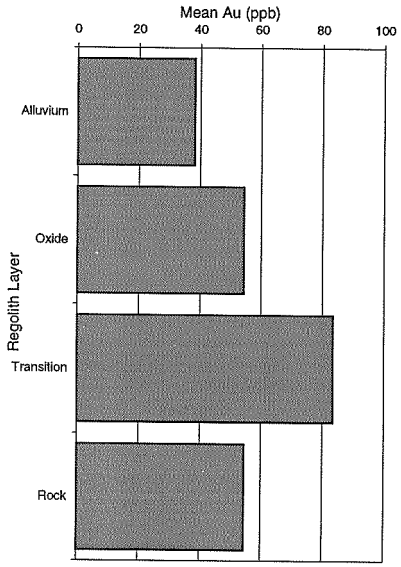

Figure 79: Mean Au for each regolith layer from the Mt Joel 0 mN prospect.

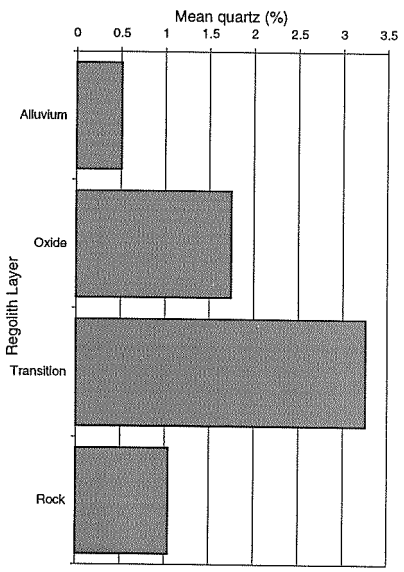

Figure 80: Mean quartz for each regolith layer from the Mt Joel 0 mN prospect.

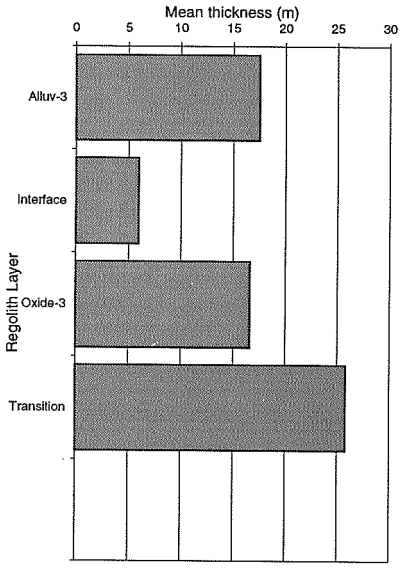

Figure 81: Mean thickness of regolith layers optimized for Au grade discrimination, from the Mt Joel 0 mN prospect.

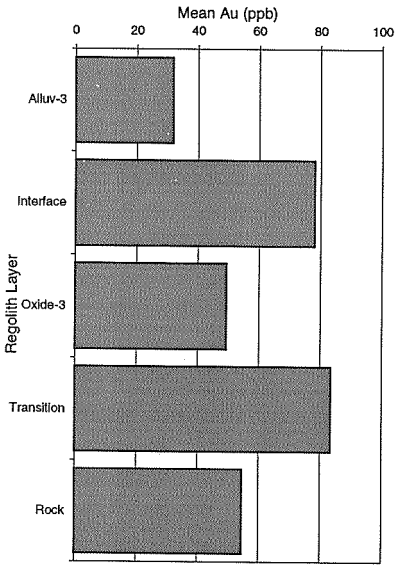

Figure 82: Mean Au for regolith layers optimized for Au grade discrimination, from the Mt Joel 0 mN prospect.

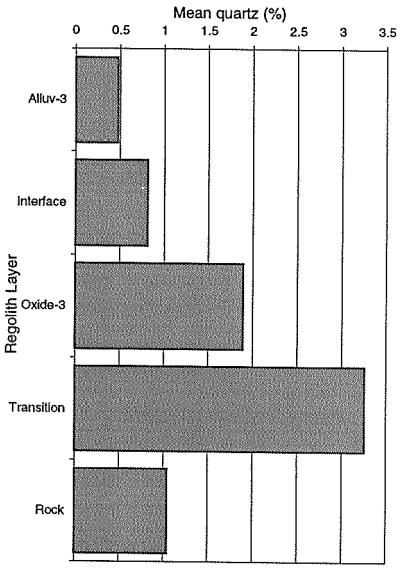

Figure 83: Mean quartz for regolith layers optimized for Au grade discrimination, from the Mt Joel 0 mN prospect.

Gold concentrations are higher directly above the weathering front (Figure 84), and at the base of complete oxidation (Figure 86), possibly due to primary variation, again supported by the similar trends for quartz (Figure 85 and Figure 87). However, calculations based on the unconformity surface (Figure 88) show a significant interface enrichment, which (as elsewhere) is not observed for quartz (Figure 89). There is a minor enhancement in the data contrast by gridding and analysing at higher resolution (Figure 90). The strong increase in the Au content of the transition at shallow depths is also clearly observed in a plot of Au concentration vs. elevation for the *in situ* material (Figure 91). Quartz content shows a very similar depth distribution (Figure 92).

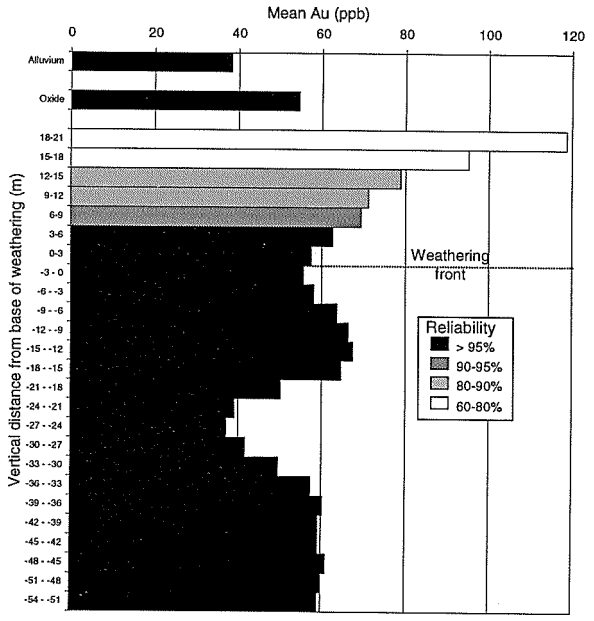

Figure 84: Mean Au vs. distance from the weathering front for the Mt Joel 0 mN prospect.

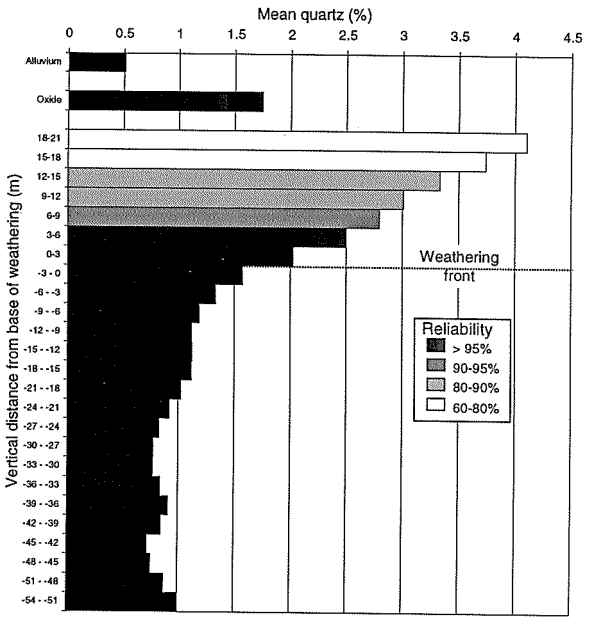

Figure 85: Mean quartz vs. distance from the weathering front for the Mt Joel 0 mN prospect.

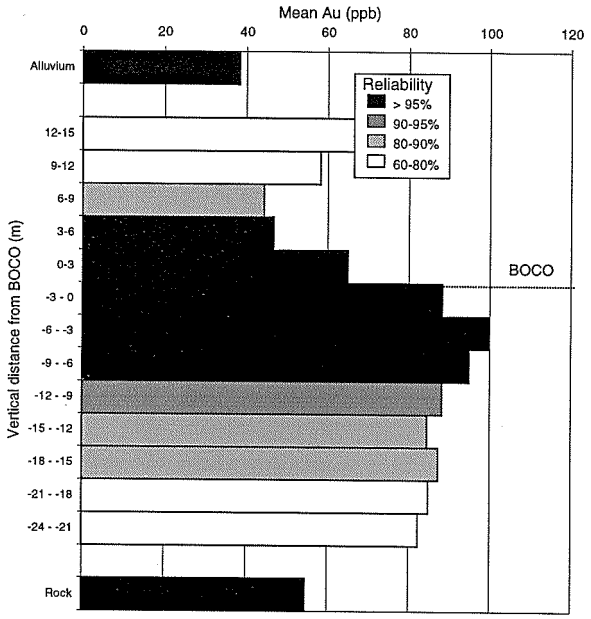

Figure 86: Mean Au vs. distance from the base of complete oxidation for the Mt Joel 0 mN prospect.

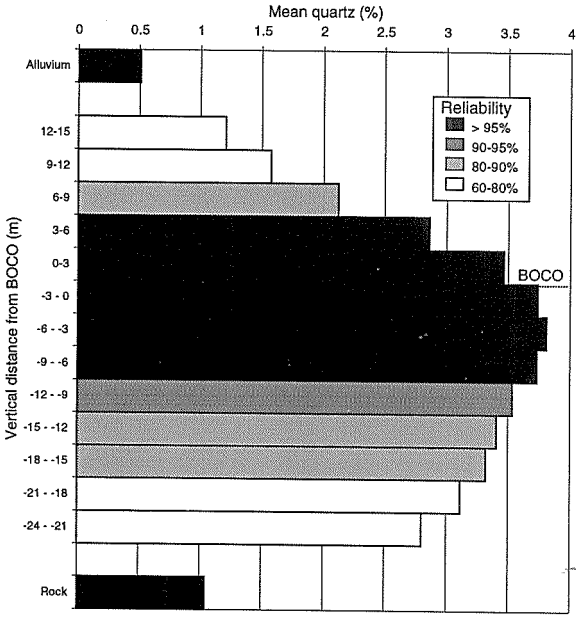

Figure 87: Mean quartz vs. distance from the base of complete oxidation for the Mt Joel 0 mN prospect.

Gold cut-off diagrams (Figure 93 (a) and (b)) indicate that the mineralization at 0 mN resembles that at 1600 mN (Figure 61 (a) and (b)), in that the Au distribution appears closely controlled by major structural factors primarily running N-S. This is also seen in the distribution of vein quartz (Figure 93 (c) and (d)). However, the Au interface anomaly (Figure 93 (a) and (b)) is more striking than at the other Mt Joel prospects.

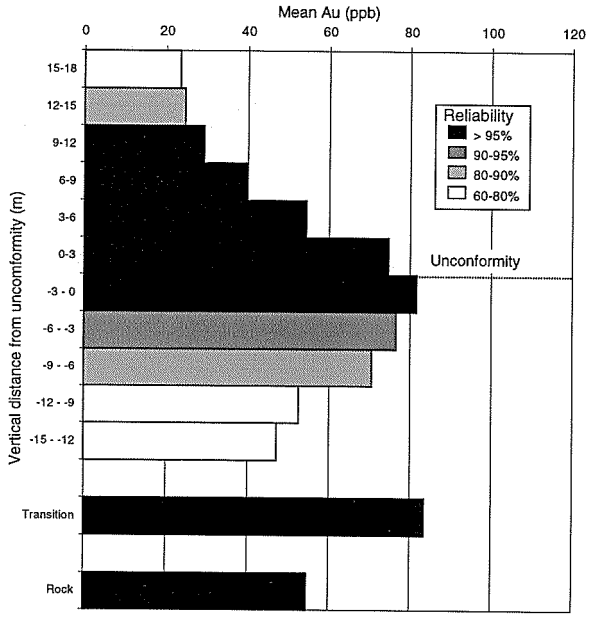

Figure 88: Mean Au vs. distance from the unconformity for the Mt Joel 0 mN prospect.

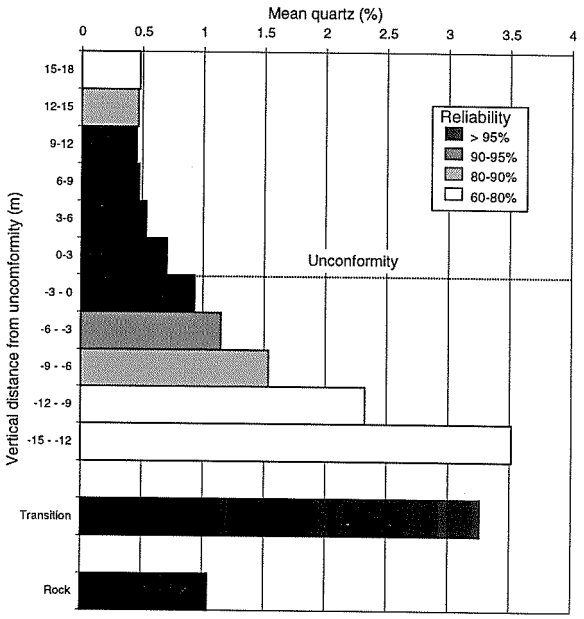

Figure 89: Mean quartz vs. distance from the unconformity for the Mt Joel 0 mN prospect.

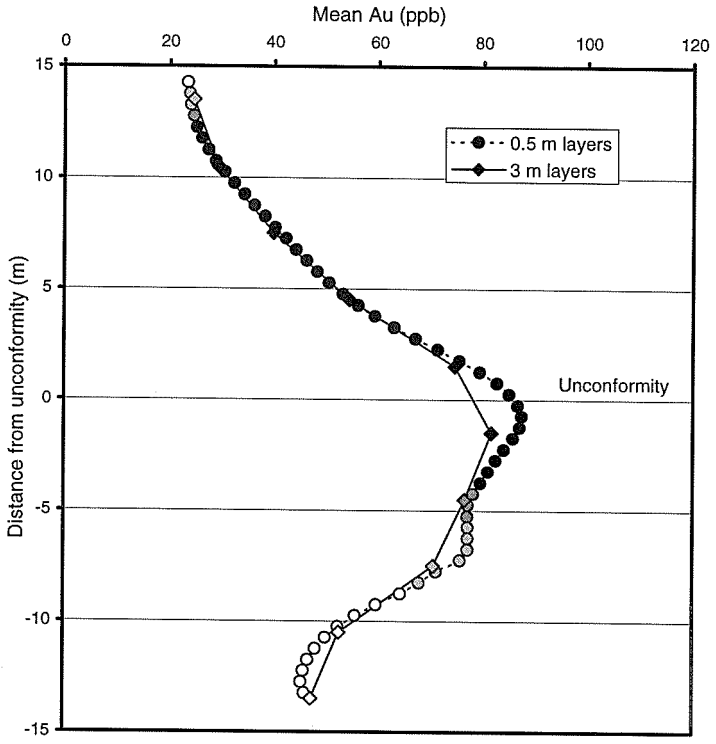

Figure 90: Mean Au vs. distance from the unconformity ("normal" and "fine" gridding) for the Mt Joel 0 mN prospect.

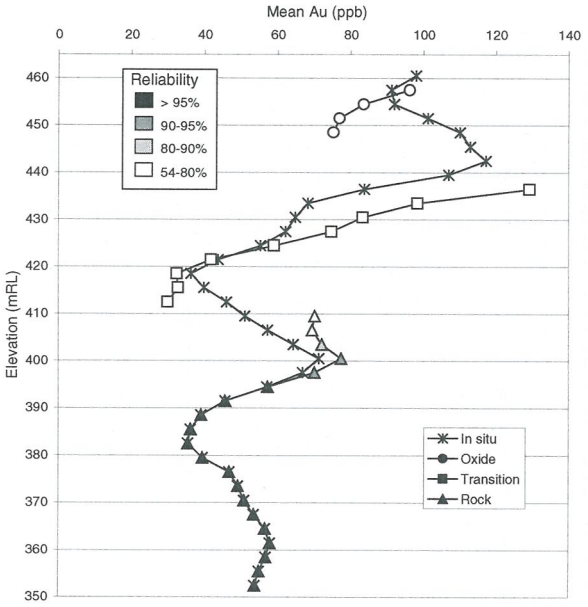

Figure 91: Mean Au vs. elevation for in situ regolith and rock at the Mt Joel 0 mN prospect.

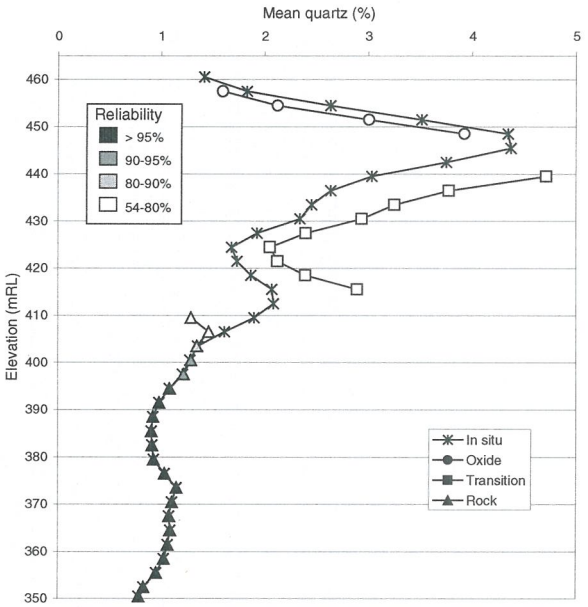

Figure 92: Mean quartz vs. elevation for in situ regolith and rock at the Mt Joel 0 mN prospect.

(a) 50 ppb Au

(b) 100 ppb Au

(c) 5% quartz

(d) 10% quartz

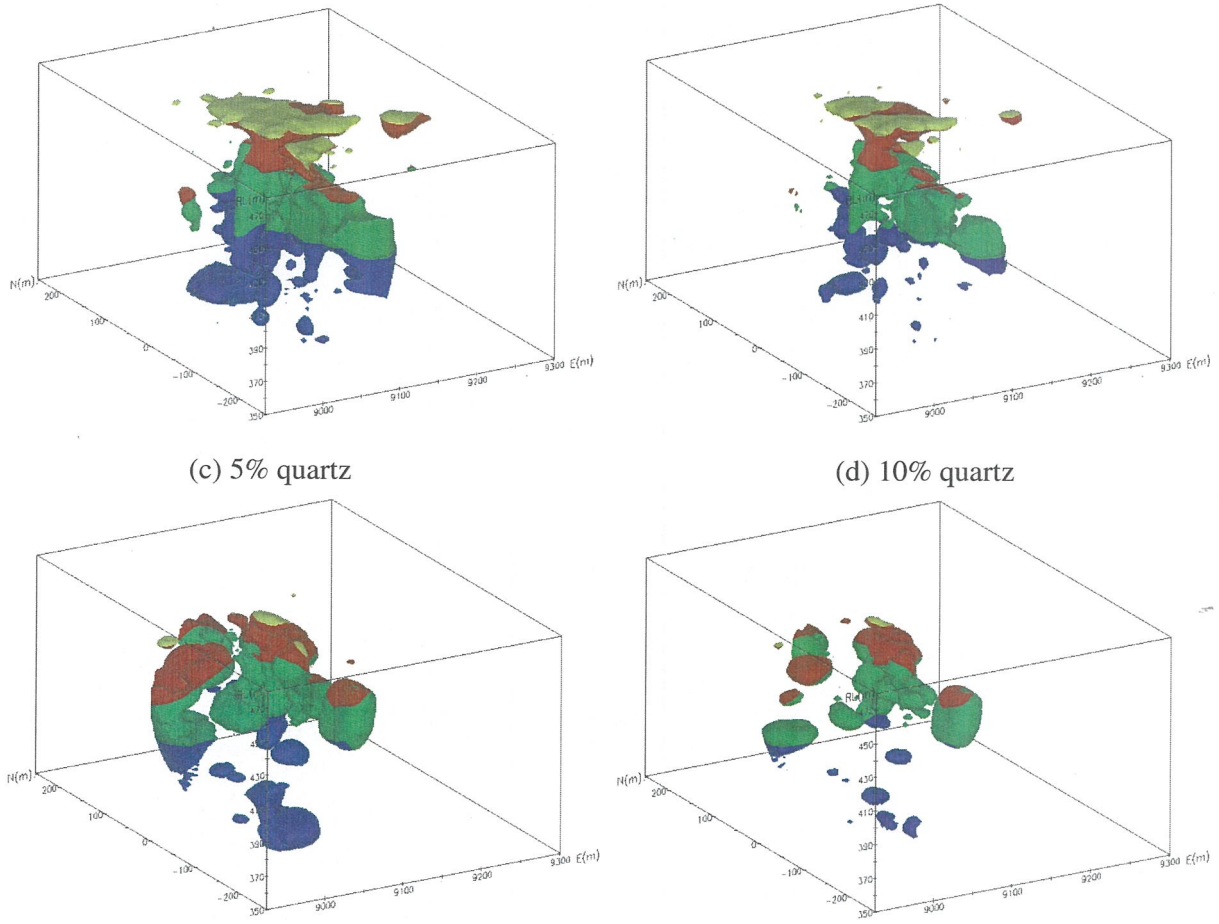

Figure 93: Gold distribution using (a) 50 ppb and (b) 100 ppb, and quartz distribution using (c) 5% and (d) 10% cut-offs for the 0 mN prospect, Mt Joel, using a 2 x vertical exaggeration. Where Au or quartz are greater than the cut-off, the material is coloured according to the regolith horizon: blue - rock, green - transition, red - oxide, yellow - transported cover.

5.7 Conclusions

Data for the 5 prospects are summarized in Tables 8 - 11. The 3000 and 2400 mN prospects have shallow alluvium, with deeper transported cover at the other sites (Table 8; Figure 94). Of the more deeply covered prospects, the 0 mN prospect has less alluvium (and less total regolith) than the 1600 and 800 mN prospects, probably because it is on the margins of the palaeochannel. Although the weathering front is deeper beneath the palaeochannel, the residuum, particularly the oxide horizon, is significantly thicker at the 2400 and 3000 mN prospects.

Table 8: Regolith horizon thicknesses for Mt. Joel

	Mean thickness (m)				
	3000	2400	1600	800	0
Alluvium	7.5	10.4	60.3	60.1	20.5
Oxide	59.9	57	26.5	33.9	19.6
Transition	26.9	24.4	30.7	18.8	25.8
Alluvium – 3m	4.5	7.4	57.3	57.1	17.5
Interface	6	6	6	6	6
"Leached zone"	19.2	35.5	4.7	-	-
Lower Oxide / Oxide	37.7	18.5	18.8	30.9	16.6
Transition	26.9	24.4	30.7	18.8	25.8

- not applicable

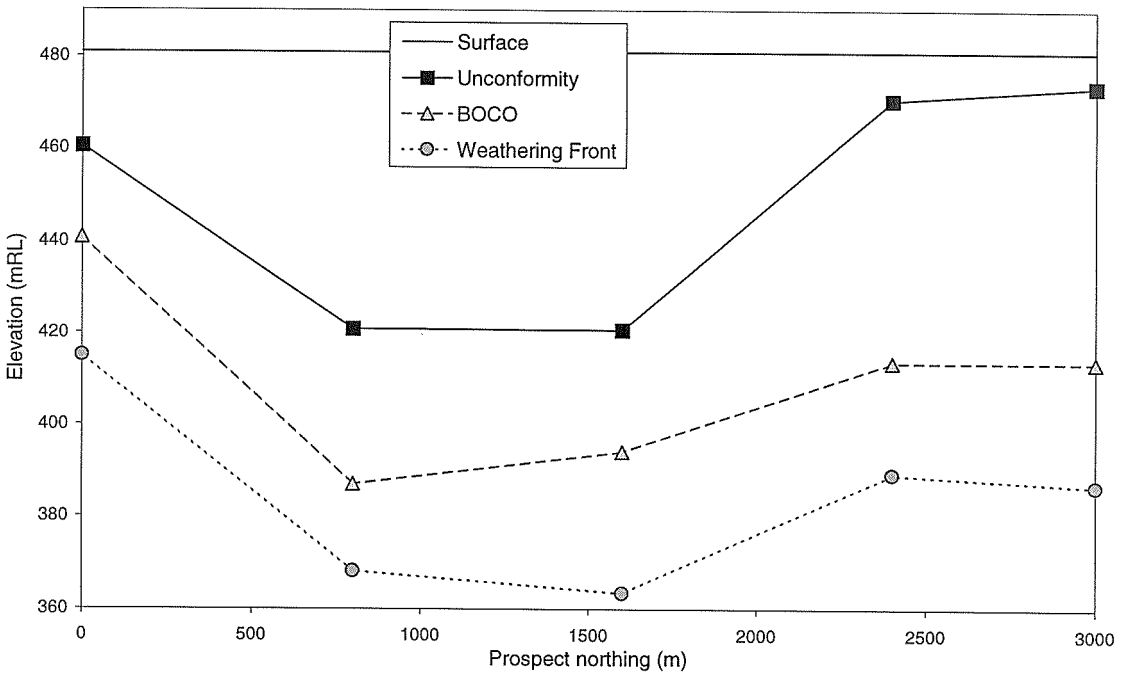

Figure 94: Regolith boundaries at Mt Joel.

Close analysis of Table 9, along with the various plots presented in Sections 5.2 - 5.6, indicates major variability in Au distribution between sites. Much of this variability is presumably related to primary variation in Au concentrations, as indicated by the close agreement with the patterns for quartz distribution for all prospects except 800 mN (Table 10). The Au concentration in the transition is

always greater than or equal to that in the rock, consistent with an residual enrichment of 1.5 – 2 times during weathering, overprinted on a variability of approximately 50%. However, because of this original variability, it is difficult to obtain reliable (as opposed to accurate) determinations of enrichment. Relative Au contents in the transition and oxide horizons are even more variable. At the 3000, 2400 and, possibly, 1600 mN prospects there is a Au-poor zone in the upper oxide, for which the lower boundary is lowering southwards (Table 11). Although at first sight, this data might suggest a depletion front that is affected by the original groundwater flow path, the similarity of results for quartz suggests that this "depletion" is primary.

Table 9: Calculated Au concentrations for regolith horizons at Mt. Joel.

Horizon	Mean Au (ppb) 3000	2400	1600	800	0
Alluvium	20	35	18	23	38
Oxide	58	65	77	76	54
Transition	101	58	133	57	84
Rock	103	38	120	42	55
Alluvium – 3 m	15	27	17	19	32
Interface	29	59	44	111	78
Au-poor oxide	27	47	53	-	-
Rest of Oxide	76	114	91	72	49
Transition	101	58	133	57	84
Rock	103	38	120	42	55
Depletion ratio (Au-poor oxide)/(Rest of oxide)	35%	42%	58% ?	-	-

- not applicable

Table 10: Calculated quartz vein contents for regolith horizons at Mt. Joel.

Horizon	Mean Au (ppb) 3000	2400	1600	800	0
Alluvium	0.7	0.8	0.6	0.5	0.5
Oxide	1.4	1.8	1.8	1.0	1.7
Transition	1.6	1.5	2.1	1.9	3.3
Rock	1.5	1.1	1.5	2.5	1.0
Alluvium – 3 m	0.6	0.9	0.5	0.5	0.5
Interface	0.7	0.6	1.3	0.6	0.8
Au-poor oxide	1.1	1.3	1.5	-	-
Rest of Oxide	1.6	3.0	1.9	1.1	1.9
Transition	1.6	1.5	2.1	1.9	3.3
Rock	1.5	1.1	1.5	2.5	1.0
Depletion ratio (Au-poor oxide)/(Rest of oxide)	66%	42%	80% ?	-	-

- not applicable

Table 11: Median elevations of regolith boundaries for Mt. Joel

Boundary	Median elevation (mRL) 3000	2400	1600	800	0
Depletion front (mRL)	450	432	414 ?	-	-
Unconformity	473	471	422	419	461
BOCO	412	417	395	388	444
Weathering front	387	390	365	368	411

- not applicable

It is of interest to note, that in the absence of quartz data, the lower Au contents of the upper oxide zone in the three northern prospects could easily be postulated to be due to weathering effects. Such effects should be taken into account in investigating other sites, particularly in areas such as the northern Yilgarn, where redistribution is commonly expected to be minor.

There is however, significant Au enrichment along the interface between transported overburden and the oxide, strongest at the 800 and 0 mN prospects (Table 9). This is presumably because the 800 and 0 mN prospects have a lateritic cover, giving rise to enrichment at the palaeosurface. The higher Au concentration in the alluvium for the 0 mN prospect is possibly due to the greater relief of the palaeosurface giving rise to contamination of exotic cover with local sources of Au.

6 DISCUSSION AND CONCLUSIONS

The Mt Joel prospect provides a useful site to test MVS calculations of Au concentration, enrichment and depletion in regolith and rock. Section 4 compares previous studies using raw data (Porto *et al.*, 1999) with MVS, checking the validity of the MVS VOLUME_AND_MASS calculations. The MVS calculations can be, and are being, used extensively (Britt and Gray, 1999; Gray, 1999; Sergeev and Gray, 1999). In contrast, raw data calculations are extremely time-consuming and only possible with well-controlled, well organized and straightforward logging schemes, such as the GCM scheme used at Mt Joel (Section 3.2). Thus, the generally excellent agreement between raw data and MVS calculations (Section 4), particularly when data are viewed as a function of depth, is very encouraging.

There are, however, differences in results between the two methods. The MVS data tend to be smoother than the raw data, probably reflecting averaging of data across the sample area. The proportionally lower concentrations for the MVS data, relative to the raw data, most probably reflect the spatial bias of the drilling. The MVS method appears less effective at defining high contrast boundaries, such as the Au-enrichment at the unconformity, although this interface enrichment is still clear. Comparison of results from "normal" gridding (2.5 m RL spacing, calculations for 3 m slices) and "fine" gridding (0.5 m RL spacing, calculations for 0.5 m slices) indicate little improvement in data quality at higher resolution. This may be partially due to problems in extrapolating regolith boundaries and Au concentrations into parts of the gridded area with low densities of drilling.

The Mt Joel prospect represents sites where (particularly for the 3000 and 2400 mN prospects) Au mineralization tends to be diffuse and there is a clear heterogeneity in the primary Au grade, making calculations of depletion and/or enrichment difficult. In addition, similarities between prospects (*e.g.*, the 3000 and 2400 mN prospects and the 800 and 0 mN prospects) provide an opportunity to cross-check hypotheses. Having indicated the MVS calculations to be accurate and comparable to raw data calculations, individual calculations for each prospect (Sections 5.2 to 5.6) and compilation of critical values (Section 5.7) show the major features to be:

(i) major vertical variability in Au concentrations commonly correlated with variation in quartz content, presumably reflecting primary variation;
(ii) approximately 1.5 – 2 x residual enrichment of Au in the transition;
(iii) a relatively Au-poor zone within the upper oxide at the 3000 and 2400 mN prospects. The base of this zone varies from 450 mRL for the 3000 mN prospect to 432 mRL for the 2400 mN prospect and, possibly, 414 mRL for the 1600 mN prospect. This variation is significantly greater than any variation in regolith boundaries between the two prospects, and appears to be primary;
(iv) a marked interface enrichment, most clearly observed for the 800 and 0 mN prospects where lateritic residuum has been retained;
(v) generally lower Au concentrations in the transported cover than in residuum. The highest Au concentrations in transported material occur in the 0 mN prospect, possibly because it is an area of greater palaeo-relief and the exotic transported material could be more readily contaminated by local sources of Au.

Thus, MVS calculations of Au concentrations within the regolith and bedrock have been demonstrated to agree well with previous calculations based on raw data. MVS calculations are also at least partially successful at determining regolith redistribution patterns of Au at a problematical site.

ACKNOWLEGMENTS

I would like to thank Great Central Mines Ltd. which has kindly provided access to the Mount Joel site and to their exploration data base. Personnel from the Yandal exploration group are greatly acknowledged for their support during field work and later analyses. Dr. Neil Phillips and Dr Jim Wright are also acknowledged for in-house discussions. Dr Charles Butt, Dr. Ravi Anand, Dr Matthias Cornelius, Mr John Wildman and Ms Allison Britt provided invaluable advice during the course of this work and preparation of this report.

REFERENCES

Britt, A.F. and Gray, D.J., 1999. Supergene gold dispersion at the Argo and Apollo deposits, Western Australia. (CRCLEME/AMIRA P504: Supergene mobilization of gold and other elements in the Yilgarn Craton). CSIRO Division of Exploration and Mining Restricted Report 639R. 51pp + accompanying CD.

Gray, D.J., 1999. Supergene gold dispersion at the Panglo gold deposit,. (CRCLEME/AMIRA P504: Supergene mobilization of gold and other elements in the Yilgarn Craton). CSIRO Division of Exploration and Mining Restricted Report 649R. 18pp + accompanying CD. .

Phillips, G.N., Vearncombe, J. R. and Eshuys, E., 1998. Yandal greenstone belt, Western Australia: 12 million ounces of gold in the 1990s. Mineralium Deposita, 33: 310-316.

Porto, C.G., Sergeev, N.B. and Gray, D.J., 1999. Gold distribution, regolith and groundwater characteristics at the Mt Joel prospect, Western Australia. (CRCLEME/AMIRA P504: Supergene mobilization of gold and other elements in the Yilgarn Craton). CSIRO Division of Exploration and Mining Restricted Report 553R. CRC LEME Restricted Report 96R, 263pp + accompanying CD.

Sergeev, N.B. and Gray, D.J., 1999. Geochemistry, hydrogeochemistry and mineralogy of regolith, Twin Peaks and Monty Dam gold prospects, Western Australia. (CRCLEME/AMIRA P504: Supergene mobilization of gold and other elements in the Yilgarn Craton). CSIRO Division of Exploration and Mining Restricted Report 643R. 151pp + accompanying CD.